

A Computational Framework for Identifiability and Ill-Conditioning Analysis of Lithium-Ion Battery Models*

Diana C. López C. and Günter Wozny

Chair of Process Dynamics and Operation, Technische Universität Berlin
Sekr. KWT-9, Str. des 17. Juni 135, D-10623 Berlin, Germany

Antonio Flores-Tlacuahuac and Ruben Vasquez-Medrano

Departamento de Ingeniería y Ciencias Químicas, Universidad Iberoamericana,
Prolongación Paseo de la Reforma 880, México D.F., 01210, México

Victor M. Zavala

Mathematics and Computer Science Division, Argonne National Laboratory
9700 South Cass Avenue, Argonne, IL 60439, USA

Abstract

Recovering kinetic, transport, and thermodynamic parameters is a key task in the development of battery models. This task is complicated because of the lack of informative experimental data and because of the complexity of the associated partial differential equation models. We present a computational framework that combines a variety of techniques to investigate the effects that different sources of experimental information on parameter identifiability and on structural ill-conditioning. We analyze the electrochemical isothermal Lithium-ion model developed and validated by Doyle et al. which consists of a lithiated-carbon anode (Li_xC_6), a polymer electrolyte, and a lithium-manganese-oxide cathode ($Li_yMn_2O_4$). We use our framework to guide the selection of experimental information. We demonstrate that the use of voltage discharge information enables the identification of a small parameter subset, regardless of the number of experiments considered. We also demonstrate that the use of electrolyte concentration information significantly aids identifiability and mitigates ill-conditioning.

Keywords: Lithium-ion batteries, parameter estimation, identifiability, ill-conditioning, partial differential equations.

*Preprint ANL/MCS-P5366-0615.

1 Introduction

There is significant interest in developing accurate Lithium-Ion (Li-Ion) battery models to perform systems design and real-time control tasks. For a review on the topic the reader is referred to [39, 18]. The development of methods for parameter estimation and structural model analysis is important because it can enable improved understanding of the physical system, it can better guide collection of experimental data, and it can ultimately enhance model predictability [43, 15, 16, 18, 24, 41, 42]. Estimating parameters and analyzing Li-ion models is challenging because of the complexity of the governing equations, their natural overparameterization, and the lack of informative experimental data [18]. This is particularly true in rigorous electrochemical-based models such as those derived from porous electrode and concentrated solution theories [11, 19, 12] which are described by complex nonlinear and coupled sets of partial differential and algebraic equations (PDAEs).

Estimation techniques characterize the performance of parameter estimates by analyzing confidence levels. Santhanagopalan et al., [40] use sensitivity analysis to guide such an analysis while Ramadesigan et al., [38] use Markov Chain Monte Carlo to have a more accurate description of the posterior distribution. Identifiability and ill-conditioning analysis techniques study the model structure by using rank analysis of the Fisher-information matrix [1, 17, 47] and of the parameter-output sensitivity matrix [1, 2, 17, 30]. These techniques have been developed and applied in many fields such as chemical reactors [21, 35, 44, 50, 51], bioprocesses [6, 30, 29, 49], and biochemical networks [8, 10]. In the context of Li-ion batteries they have been applied to models of different complexity that span linear and nonlinear equivalent-circuit models [42, 24] to rigorous models [15, 16, 41]. These studies address identifiability and ill-conditioning from different angles: some studies seek to reduce the model and restrict the parameter space [24], some studies seek to detect unidentifiable parameters using variance information [41], and some other studies seek to detect unidentifiable parameters using rank and eigenvalue analysis [42, 15, 16].

Few studies analyze connections between estimator performance and model structure. This is important because structural model issues can significantly distort conclusions obtained with traditional estimation studies. For instance, the studies in [15, 42] note the influence of small eigenvalues of the Fisher-information matrix on parameter variances but no in-depth study is performed. In [39] the authors note significant ill-conditioning of the Jacobian of the differential algebraic equation (DAE) system resulting from discretization of the PDAEs but do not analyze the effect of such ill-conditioning on parameter estimates. In [42] the authors study a nonlinear equivalent-circuit model and recognize the inaccuracies of approximating the parameter covariance matrix using an ill-conditioned Fisher-information matrix. Some studies have also proposed to monitor the eigenvalues of the Hessian matrix of the estimation problem to diagnose identifiability issues but do not analyze specific sources of the ill-conditioning [53, 31].

Identifiability and ill-conditioning analysis can also aid selection of appropriate experimental information. In the context of Li-Ion batteries, Schmidt et al., [41] note that identifiability was improved when multiple voltage discharge curves were used for estimation but such information did not make the entire parameter set identifiable. The authors do not provide an explanation for this. Although the idea of including more experimental information is fairly intuitive, there are currently no frame-

works that enable a systematic assessment and diagnosis of ill-conditioning and identifiability issues in Li-ion battery models and that can better guide experimental data collection.

In this work we present a computational framework to perform estimation, ill-conditioning, and identifiability analysis of Li-Ion batteries. To illustrate the capabilities of our framework, we use the electrochemical isothermal Li-ion model originally proposed and validated by Doyle et al. [11, 19, 12]. The Li-ion battery analyzed consists of a lithiated-carbon anode (Li_xC_6), a polymer electrolyte, and a lithium-manganese-oxide-spinel cathode ($Li_yMn_2O_4$). We evaluate estimator performance using approximate covariance matrices obtained from the parameter-output sensitivity matrix and Monte Carlo simulations. We use singular value decomposition (SVD) of the parameter-output sensitivity matrix to diagnose and determine the sources of ill-conditioning and we use a variance-decomposition technique that determines the influence of small singular values on specific parameters. We perform QR and SVD decompositions to rank and determine identifiable and unidentifiable parameters. We also use dynamic sensitivity profiles to assess the excitation provided by different parameters on different outputs. We illustrate how to combine all of these techniques to assess the impact of different sources of experimental information and we demonstrate that the use of voltage profiles is only sufficient to estimate a small parameter subset. We then demonstrate that a single measurement of electrolyte concentration is sufficient to determine a much larger parameter subset that includes all the parameters under study except one. Sensitivity profiles indicate that this last parameter does not sufficiently excite the model outputs.

The paper is organized as follows. We first present the different components of the computational framework to evaluate estimator performance, ill-conditioning, and identifiability of nonlinear models by using sensitivity and Monte Carlo methods. We then give an overview of the governing equations of the Li-ion model of Doyle et al. [11, 19, 12]. We then present a case study to illustrate the use of our framework. We conclude by summarize our findings and providing directions for future work.

2 Computational Framework

In this section we describe the different techniques of the computational framework. The combination of these techniques will enable us to assess estimator performance as well as to perform ill-conditioning and identifiability analysis. We start with basic notation and then discuss two major paradigms used for analysis: I) Numerical techniques that perform singular value analysis of the so-called sensitivity matrix and II) Statistical techniques based on Monte Carlo simulations to estimate the parameter covariance matrix and quantify uncertainty. For each paradigm, we provide different methods to diagnose ill-conditioning and identifiability issues.

2.1 Definitions and Notation

We assume a dynamic model is described by the differential and algebraic equation (DAE) system,

$$\dot{x}(t) = f(x(t), z(t), u(t), \theta) \quad (2.1a)$$

$$0 = g(x(t), z(t), u(t), \theta) \quad (2.1b)$$

$$y(t) = h(x(t), z(t)) \quad (2.1c)$$

$$x(t_0) = x_0, \quad (2.1d)$$

where $t \in \mathfrak{R}$ is the independent time variable, $x(t) \in \mathfrak{R}^{N_x}$ and $z(t) \in \mathfrak{R}^{N_z}$ are the differential and algebraic state variables, respectively; $u(t) \in \mathfrak{R}^{N_u}$ are the time-varying input signals (i.e., experiment design vector or controls), and $\theta \in \mathfrak{R}^{N_\theta}$ is the unknown parameter vector. The differential $f(\cdot) : \mathfrak{R}^{N_x} \times \mathfrak{R}^{N_z} \times \mathfrak{R}^{N_u} \times \mathfrak{R}^{N_\theta} \rightarrow \mathfrak{R}^{N_x}$ and algebraic $g(\cdot) : \mathfrak{R}^{N_x} \times \mathfrak{R}^{N_z} \times \mathfrak{R}^{N_u} \times \mathfrak{R}^{N_\theta} \rightarrow \mathfrak{R}^{N_x}$ mappings are assumed to be twice continuously differentiable in all their arguments. The initial conditions of the DAE system (2.1a)-(2.1b) are denoted by (x_0, z_0) and we say that these are consistent if they satisfy $0 = g(x_0, z_0, u_0, \theta)$ for fixed u_0 and θ .

We consider a vector of response variables $y(t) \in \mathfrak{R}^{N_y}$ given by the mapping $h(\cdot) : \mathfrak{R}^{N_x} \times \mathfrak{R}^{N_z} \rightarrow \mathfrak{R}^{N_y}$ (2.1c) which we also assume to be twice continuously differentiable. We denote the i -th entry of vector $y(\cdot)$ as $y^{(i)}(\cdot)$. We establish a set of time measurement points $\mathcal{T} = \{t_1, \dots, t_{N_m}\}$ and a set of experiments $\mathcal{E} := \{\xi_1, \dots, \xi_{N_e}\}$. Each experiment $\xi \in \mathcal{E}$ has a corresponding input signal $u_\xi \in \mathfrak{R}^{N_e}$ and responses $y_\xi(u_\xi, \theta, t) \in \mathfrak{R}^{N_y}$, $t \in \mathcal{T}$, $\xi \in \mathcal{E}$. The inputs are collected in the vector $u := (u_{\xi_1}, \dots, u_{\xi_{N_e}})$ and the model responses are collected in the vector

$$Y(u, \theta) := (y_{\xi_1}(u_{\xi_1}, \theta, t_1), \dots, y_{\xi_1}(u_{\xi_1}, \theta, t_{N_m}), \dots, y_{\xi_{N_e}}(u_{\xi_{N_e}}, \theta, t_1), \dots, y_{\xi_{N_e}}(u_{\xi_{N_e}}, \theta, t_{N_m})) \in \mathfrak{R}^{N_y \cdot N_m \cdot N_e}. \quad (2.2)$$

We define the corresponding set of observed (measured) response vector as $\bar{Y} \in \mathfrak{R}^{N_y \cdot N_m \cdot N_e}$. We use $\hat{\theta} \in \mathfrak{R}^{N_\theta}$ to denote the model parameter vector estimated from the observed data \bar{Y} . We assume that this is obtained by solving the maximum likelihood problem [2],

$$\hat{\theta} := \arg \min_{\theta} \Phi(u, \theta) \quad (2.3)$$

where,

$$\Phi(u, \theta) := \frac{1}{2} (Y(u, \theta) - \bar{Y})^T C_y^{-1} (Y(u, \theta) - \bar{Y}). \quad (2.4)$$

The true value of the parameter vector is denoted as $\theta^* \in \mathfrak{R}^{N_\theta}$. We assume output measurement errors that are uncorrelated among outputs and experiments. This implies that $\bar{y}_\xi^{(i)}(t) = y_\xi^{(i)}(u_\xi, \theta^*, t) + \epsilon^{(i)}$ where $\epsilon^{(i)} \sim \mathcal{N}(0, \sigma_y^{(i)})$ for $i = 1, \dots, N_y$, $t \in \mathcal{T}$, and $\xi \in \mathcal{E}$. Under these assumptions the measurement covariance matrix $C_y \in \mathfrak{R}^{N_y \cdot N_m \cdot N_e \times N_y \cdot N_m \cdot N_e}$ is diagonal with entries given by the variances $(\sigma_y^{(i)})^2$. We also define $\Sigma_y := C_y^{1/2} \in \mathfrak{R}^{N_y \cdot N_m \cdot N_e \times N_y \cdot N_m \cdot N_e}$ as the measurement standard deviation matrix which implies that $Y(u, \theta) \sim \mathcal{N}(\bar{Y}, \Sigma_y)$. Finally, we define the parameter covariance matrix,

$$C := \mathbb{E} \left[(\hat{\theta} - \theta^*)(\hat{\theta} - \theta^*)^T \right], \quad (2.5)$$

where the expectation $\mathbb{E}[\cdot]$ is taken with respect to the distribution $\mathcal{N}(\bar{Y}, \Sigma_y)$ [2].

We also define the parameter-output sensitivity matrix

$$S := \nabla_{\theta} Y(u, \hat{\theta}) \in \mathfrak{R}^{N_y \cdot N_m \cdot N_e \times N_{\theta}}, \quad (2.6)$$

and the Fisher-Information matrix,

$$F := S^T C_y^{-1} S \in \mathfrak{R}^{N_{\theta} \times N_{\theta}}. \quad (2.7)$$

2.2 Analysis Paradigms

We now describe two paradigms to analyze estimated parameters and identify structural issues. The first paradigm uses sensitivity information to form the Fisher-information matrix which in turn can be used to approximate the parameter covariance matrix. The second paradigm approximates the covariance matrix via Monte Carlo.

2.2.1 Sensitivity Method

We solve the parameter estimation problem (2.3) to obtain the parameter estimate $\hat{\theta}$, the sensitivity matrix S , and the Fisher-information matrix. We compute an approximate covariance matrix C using the inverse of the Fisher matrix which is in turn obtained from S . The sensitivity-based method is straightforward to implement and provides fast local information of the model behavior around the parameter estimates. Sensitivity information can also be used in conjunction with singular value decomposition to perform structural model analysis. Because of its inherent local nature, however, the covariance matrix obtained from sensitivity might not provide a good covariance approximation (specially true when S is ill-conditioned). Consequently, this method is most useful for qualitative analysis.

2.2.2 Monte Carlo Method

In this setting we obtain L replications of the observations \bar{Y}_j , $j = 1, \dots, L$ obtained by sampling $\mathcal{N}(\bar{Y}, \Sigma_y)$. For each observation \bar{Y}_j we solve problem (2.3) to obtain the estimates $\hat{\theta}_1, \dots, \hat{\theta}_L$. This information is used to compute the approximate covariance matrix C and confidence intervals of each parameter. The replications can also be interpreted as perturbations on the data that can help us to assess the stability of the estimates. When the true parameter θ^* is known (as in theoretical studies) we can also assess the accuracy of the estimator by computing the bias and the empirical mean squared error of the estimate. The Monte Carlo approach enables a more quantitative analysis but it is computationally demanding.

2.3 Estimator Analysis

To assess the performance of an estimator we can use precision or accuracy arguments which we now describe.

2.3.1 Estimator Precision

The precision of the estimator $\hat{\theta}$ can be assessed by using an approximate covariance matrix C [2, 14, 27, 49]. This is a matrix whose (i, j) -element σ_{ij}^2 is the variance of the i -th parameter $\hat{\theta}^{(i)}$ with respect to the j -th parameter $\hat{\theta}^{(j)}$ for $i, j = 1, \dots, N_\theta$. The diagonal element σ_{jj}^2 is the variance of the j -th parameter $\hat{\theta}^{(j)}$. With the results of C we calculate the confidence interval for each parameter. Our framework considers two strategies to compute the covariance matrix.

Covariance Based on Sensitivity Matrix. In this approach, the covariance matrix C is approximated by the *inverse* of the Fisher-information matrix which we denote as F ,

$$C \approx F^{-1} = (S^T C_y^{-1} S)^{-1}. \quad (2.8)$$

The Fisher-information matrix F can only be guaranteed to be positive definite when the sensitivity matrix S is full-rank [36]. The relationship between the Fisher matrix and the covariance matrix is derived by applying a first-order Taylor expansion of the maximum likelihood function around $\hat{\theta}$, assuming a Gauss-Newton approximation of the Hessian matrix, and by using the Cramer-Rao bound [2, 14, 27]. The Fisher matrix is also known as the average estimated covariance matrix [2]. The sensitivity matrix S can be computed either by finite differences or by integrating the system model along with the so-called sensitivity equations [3, 32, 45].

In the definition of C given in (2.8), we require matrix and inverse operations with the sensitivity matrix S . These computations could lead to significant numerical errors when the sensitivity matrix is not full-rank (i.e., it is ill-conditioned). This ill-conditioning introduces degeneracies to the eigen-system of C which in turn reflects in large parameter variances [29]. To deal with this issue, we can directly compute C based on a singular value decomposition (SVD) of the sensitivity matrix S where S is scaled as $S \leftarrow \Sigma_y^{-1} S$. SVD gives a decomposition of the form

$$S = U S_v V^T = \sum_{i=1}^{N_\theta} u_i \varsigma_i v_i^T \quad (2.9)$$

where $U \in \mathfrak{R}^{N_y \cdot N_m \cdot N_e \times p}$ and $V \in \mathfrak{R}^{N_\theta \times p}$ are orthogonal matrices with $p = \min\{N_y \cdot N_m \cdot N_e, N_\theta\}$ (we assume the typical situation in which $p = N_\theta$). Matrix $S_v := \text{diag}(\varsigma_1, \dots, \varsigma_p)$ is the singular value matrix and ς_i is i -th singular value of S . The set of singular values of S is known as the singular value spectrum (SVs). We assume the SVs to be ordered as $\varsigma_1 \geq \dots \geq \varsigma_{N_\theta} \geq 0$. The ratio of the largest and smallest singular values of S is the condition number $\kappa(S)$. The inverse of the smallest singular value of S is the collinearity index $\gamma(S)$. When one or more of the singular values approaches zero we say that the matrix S is not numerically of full-rank. The vectors $u_i \in \mathfrak{R}^{N_y \cdot N_m \cdot N_e}$ and $v_i \in \mathfrak{R}^{N_\theta}$ are the left and right singular vectors of S . Matrix C in (2.8) can be computed as

$$C = \sum_{i=1}^{N_\theta} \frac{v_i v_i^T}{\varsigma_i^2} \quad (2.10)$$

The parameter variance σ_{jj}^2 of the j -th parameter of $\hat{\theta}$ can be computed as

$$\sigma_{jj}^2 = \sum_{i=1}^{N_\theta} \frac{v_i^{(j)} \cdot v_i^{(j)}}{\varsigma_i^2} \quad (2.11)$$

where $v_i^{(j)}$ is the j -th entry of v_i for $k = 1, \dots, N_\theta$. Note that multiple singular values can contribute to the variance of parameter j . Moreover, the variances increase as the singular values decrease and this establishes a connection between structural ill-conditioning and estimator performance. The SVD decomposition approach is numerically more stable than the direct computation (2.8), particularly when S is ill-conditioned.

Covariance Based on Monte Carlo. We compute C using the estimates $\hat{\theta}_j$, $j = 1, \dots, L$ as

$$C = \frac{1}{(L-1)} \sum_{j=1}^L (\hat{\theta}_j - \mathbb{E}[\hat{\theta}])(\hat{\theta}_j - \mathbb{E}[\hat{\theta}])^T \quad (2.12)$$

where $\mathbb{E}[\hat{\theta}]$ is approximated using the sample average

$$\mathbb{E}[\hat{\theta}] \approx \frac{1}{L} \sum_{j=1}^L \hat{\theta}_j. \quad (2.13)$$

This statistical approach can better capture the effect of nonlinearities on the posterior distribution of the parameters but does not provide much insight on specific sources of identifiability issues.

Confidence Intervals. The confidence interval of the j -th parameter is given by $\theta_L^{(j)} \leq \hat{\theta}^{(j)} \leq \theta_U^{(j)}$ and this describes a range of values within which one can be confident that the corresponding true parameter $(\theta^*)^{(j)}$ lies. The limits $\theta_L^{(j)}$ and $\theta_U^{(j)}$ are computed as

$$\theta_L^{(j)} = \hat{\theta}^{(j)} - (\sigma_{jj})t_{\alpha/2, N_y \cdot N_m \cdot N_e - N_\theta} \quad (2.14a)$$

$$\theta_U^{(j)} = \hat{\theta}^{(j)} + (\sigma_{jj})t_{\alpha/2, N_y \cdot N_m \cdot N_e - N_\theta}. \quad (2.14b)$$

Here, $t_{\alpha/2, N_y \cdot N_m \cdot N_e - N_\theta}$ is the critical value of the Student's t-distribution for the given confidence level α and $N_y \cdot N_m \cdot N_e - N_\theta$ are the degrees of freedom; σ_{jj} is the standard deviation of $\hat{\theta}^{(j)}$ computed as the squared root of the j -th diagonal element of C . In the sensitivity approach $\hat{\theta}^{(j)}$ is the parameter estimate value, while in the Monte Carlo approach, we use the sample average (2.13). We also define the confidence length $\theta_U^{(j)} - \theta_L^{(j)}$ and we note that it is often convenient to express this length relative to the estimated value as $100 \cdot (\theta_U^{(j)} - \theta_L^{(j)})/\hat{\theta}^{(j)}$.

2.3.2 Estimator Accuracy

Accuracy of a parameter estimate is often evaluated using the bias,

$$\beta(\hat{\theta}) = \mathbb{E}[\hat{\theta}] - \theta^*. \quad (2.15)$$

The bias quantifies the difference to be expected between an estimator and the true or reference value. An estimator based on a finite sample, however, can additionally be expected to differ from the true parameter due to the randomness in the sample. One measure that is used to reflect these two effects is the mean square error (MSE),

$$MSE = \|\beta(\hat{\theta})\|^2 + \text{Tr}[\text{Var}(\hat{\theta})]. \quad (2.16)$$

The first term on the right-hand side is the squared norm of the bias and the second term is the trace of the variance. The variance arises from the variability generated by measurement errors. We can approximate the variance as $\text{Tr}[\text{Var}(\hat{\theta})] \approx \text{Tr}[C] = \text{sum}(\text{diag}(C))$ [23, 33]. Consequently, an ideal estimator seeks to minimize the variance of the parameter estimates and the bias. In fact, the trace of the variance $\text{Tr}[\text{Var}(\hat{\theta})]$ is the A-optimality criterion used in optimal experimental design [36]. We highlight that our maximum likelihood problem does not use prior information because this would introduce an additional bias to our estimates. We also avoid the use of prior information to assess identifiability issues in a more systematic manner.

2.4 Structural Analysis

The previous techniques seek to analyze estimator performance by computing parameter variances, confidence intervals, biases, and MSEs. Such techniques by themselves, however, do not identify sources of ill-conditioning resulting from structural deficiencies of the parameter covariance and Fisher matrices [1, 10, 17, 26, 44, 47]. Our objective in this section is to exploit the connection between the eigenvalues of F and C with the singular values of the sensitivity matrix S to identify the presence and sources of ill-conditioning [28]. The rationale is that, if certain parameters of $\hat{\theta}$ are unidentifiable, some columns of the sensitivity matrix S are linearly dependent (i.e., S is not of full-rank) which implies that F and C are singular or nearly singular [10, 25, 29, 44]. Columns of S that are nearly linear dependent are a typical source of poor estimator performance [5, 29]. We thus try to identify if S is ill-conditioned by computing its rank and collinearity index, we determine which columns of S are dependent, and we analyze how small singular values influence parameter variances. We do this by analyzing matrix C and by analyzing S using SVD and QR decompositions. These procedures ultimately result in *parameter rankings* that we use to determine unidentifiable parameters under different sources of experimental information. These rankings can be used to provide recommendations for regularization and design of priors [29].

2.4.1 Ill-Conditioning Analysis

We follow the procedure for linear estimation presented by Belsley [5] and modified for nonlinear models in [29]. The procedure is summarized as follows:

1. Perform SVD of S to obtain SVs $\{\varsigma_1, \dots, \varsigma_{N_\theta}\}$.
2. Compute the condition number $\kappa(S) = \varsigma_1/\varsigma_{N_\theta}$ and collinearity index $\gamma(S) = 1/\varsigma_{N_\theta}$.
3. Check if $\kappa(S)$ and $\gamma(S)$ satisfy $\kappa(S) \leq \kappa^{max}$ or $\gamma(S) \leq \gamma^{max}$. Empirical thresholds of $\kappa^{max} = 1000$ and $\gamma^{max} = 15$ are typically used [21, 6, 30, 29]. If false, we say that S is ill-conditioned.
4. Analyze ill-conditioning of S (i.e., rank-deficiency or ill-determined rank class). A rank-deficient S has a large gap between large and small singular values limited by a ϵ -threshold. An ill-determined rank problem has SVs gradually decaying to zero without a gap between singular values. The ϵ -threshold (the lowest bound on the SVs), is defined as $\epsilon = \max\{\varsigma_1/\kappa^{max}, 1/\gamma^{max}\}$.

Singular values above the ϵ -threshold are said to be well-conditioned and those below are said to be ill-conditioned. The number well-conditioned singular values reveals the numerical rank r_ϵ of S , which ideally should be N_θ .

We highlight that the above approach relies on the definition of the thresholds $\kappa^{max}, \gamma^{max}$, which are a subjective choice. This procedure, however, provides a quantitative approach to perform comparisons among different estimators and thus evaluate the impact of different sources of information.

2.4.2 Identifiability Analysis

We now discuss techniques to detect unidentifiable parameters based on parameter variances, based on SVD of the sensitivity matrix S , and based on QR decompositions of sensitivity matrix S (also called parameter subset selection or orthogonalization method). Each technique constructs an identifiable ranking list based on different metrics. We also connect identifiability techniques with the structural ill-conditioning techniques previously discussed.

Variance Method. We can define identifiable parameters as those with variances within some given ranges [48]. We use the following simple procedure:

1. Compute C either from the Fisher-information as shown in (2.8) or (2.10) or from Monte Carlo as shown in (2.12). Take the diagonal elements of C as variances σ_{jj}^2 for each parameter with $j = 1, \dots, N_\theta$. Rank parameters in $\hat{\theta}$ by ascending order according to parameter variances.
2. Define the maximum variance ρ^{max} . Parameters above the threshold (i.e., $\sigma_{jj}^2 > \rho$) are considered unidentifiable.

SVD Method. As seen in the SVD analysis of Section 2.4.1 and in the variance-decomposition in (2.11), small (ill-conditioned) singular values inflate parameter variances. We can rank parameters by identifying singular values of S instead of variances. The following procedure relies on a variance-decomposition that quantifies the contribution of each singular value to the variance of each parameter. To perform this decomposition, the variance σ_{jj}^2 of the j -th parameter $\hat{\theta}^{(j)}$ is obtained according to (2.11). For each parameter j , we compute the proportions $\pi_{i,j} = \left[v_i^{(j)} \cdot v_i^{(j)} / \varsigma_i^2 \right] / \sigma_{jj}^2$ of the contributions of each ill-conditioned singular value ς_i , $i = r_\epsilon + 1$ to the variance σ_{jj}^2 . The rationale behind this ranking is that *ill-conditioned singular values have large contributions to parameters with large variance*. In other words, a parameter that is strongly influenced by ill-conditioned singular values provides evidence of identifiability issues. The procedure is:

1. Compute C from SVD according to (2.10) and obtain variances σ_{jj}^2 for $j = 1, \dots, N_\theta$. Perform procedure of Section 2.4.1 to obtain the ill-conditioned singular values ς_i , $i = r_\epsilon + 1$ and the numerical rank r_ϵ .
2. Compute the variance-decomposition proportion $\pi_{i,j}$, $i = r_\epsilon + 1$ for each parameter j .

3. Rank parameters of $\hat{\theta}$ by ascending ordering according to the sum of their proportions $\sum_{i=r_\epsilon+1}^{N_\theta} \pi_{i,j}$. Parameters on the top of the list are not strongly influenced by ill-conditioned singular values.
4. Define the maximum proportion threshold π^{max} (typically set to 0.5). The identifiable parameters are those satisfying $\sum_{i=r_\epsilon+1}^{N_\theta} \pi_{i,j} \leq \pi^{max}$. If $r_\epsilon = N_\theta$ then all parameters are identifiable.

QR Method. This method selects the subset of linearly independent parameters based on orthogonal projections of the columns of S [26, 30, 29]. This method is also called parameter subset selection and is a popular way of determining unidentifiable parameters. Other studies dedicated to parameter subset selection can be found in [6, 7, 8, 9, 20, 30, 35, 46, 50, 51]. The rationale behind this ranking is that the unidentifiable parameters are expected to have the largest variance among the whole parameter vector and *this can be detected by identifying the linearly dependent columns of S* . The procedure is:

1. Perform procedure of Section 2.4.1 to obtain the numerical rank r_ϵ . The dimension of the identifiable parameter subset is r_ϵ .
2. Apply a QR decomposition with pivoting (QRP) to S to obtain $S \cdot \Pi = Q \cdot R$ where Π is a permutation matrix. This matrix reorders the columns of S according to their linear dependence.
3. Build the identifiable ranking list $\tilde{\theta} = \Pi^T \hat{\theta}$.
4. Select the unidentifiable parameters as the last $(N_\theta - r_\epsilon)$ entries of ordered $\tilde{\theta}$.

3 Li-ion Battery Model

The Li-ion battery model under study is that proposed by Doyle et al. [11] and was experimentally validated by Doyle et al. in [12]. The Li-ion cell sandwich in Figure 1 consists of a lithiated carbon anode (Li_xC_6), a polymer electrolyte, and a lithium-manganese-oxide-spinel cathode ($Li_yMn_2O_4$). The active material in the composite electrodes is assumed to be made up of spherical particles and supported on an inert material. The polymer electrolyte in the separator uses a $LiPF_6$ salt in a non-aqueous liquid mixture of ethylene carbonate and dimethyl carbonate with a random co-polymer matrix of vinylidene fluoride and hexafluoropropylene. The lithium ions (Li^+) travel through the electrolyte from one porous electrode to the other whereas the electrons travel through an external closed circuit. The Li^+ ions react and diffuse in the electrodes towards the inner regions of metal oxide active material particles (the solid phase). The discharge process takes place when Li^+ ions diffuse from the anode to the cathode.

The governing equations presented in [11, 12] are based on the porous electrode and concentrated electrolyte theories. These equations consist of mass transport balances in the electrolyte including migration, diffusion, and reaction; Ohm's law in the electrolyte which includes the diffusion potential and the variation of the electrolyte resistivity with concentration; Fick's laws in the solid active material which assumes a constant solid diffusion coefficient; Ohm's law in the solid electrode matrix;

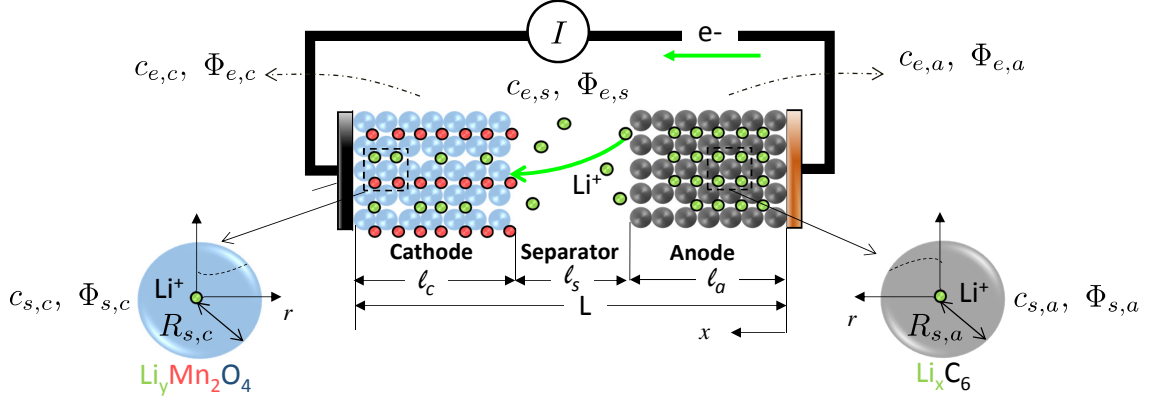


Figure 1: Li-ion cell during discharge process. Cell consists of a Li_xC_6 negative electrode, a $Li_yMn_2O_4$ positive electrode, and a separator with $LiPF_6$ salt-based electrolyte.

Butler-Volmer kinetics; and current conservation. Radial diffusion is considered to be the transport mechanism of Li^+ ions into the spherical particles in the electrodes.

The space-time model is comprised of a set of highly complex partial differential and algebraic equations. Strategies to simplify the model are discussed in [37]. We use the subscripts a , s , and c to denote anode, separator, and cathode regions, respectively. The subscripts e and s denote the electrolyte and solid phases, respectively. Three independent variables (axial coordinate x , radial coordinate r and time t) are considered. The model includes twenty dependent variables (states) summarized in Table 1 and given by,

- The electrolyte concentration $c_{e,k}(x, t)$, electrolyte potential $\Phi_{e,k}(x, t)$, and local current density $i_k(x, t)$ in all regions $k = \{a, s, c\}$.
- The solid concentration $c_{s,k}(x, r, t)$, solid potential $\Phi_{s,k}(x, t)$, and reaction rate $j_{n,k}(x, t)$ in the electrodes $k = \{a, c\}$.
- The conductivity of the electrolyte $\kappa_{0,k}(x, t)$ in all regions $k = \{a, s, c\}$.
- The open-circuit potential $U_k(x, t)$ in the electrodes $k = \{a, c\}$.

The kinetic and transport parameters to be estimated are presented in Table 2. There are the Li^+ diffusion coefficient in the solid particle of the anode $D_{s,a}$, the Li^+ diffusion coefficient in the solid particle of the cathode $D_{s,c}$, the salt diffusion coefficient in the electrolyte D , the reaction rate constant in the anode k_a , the reaction rate constant in the cathode k_c , the Bruggeman coefficient p , the film resistance at the anode R_f , and the transport number t_+ . The design and operating variables, constants and fixed parameters are summarized in Table 3.

Table 1: Variables in Li-Ion Model.

Variable	Description	Unit	Anode	Separator	Cathode
			($k = a$)	($k = s$)	($k = c$)
$c_{e,k}(x, t)$	Electrolyte concentration in region k	mol m^{-3}	✓	✓	✓
$\Phi_{e,k}(x, t)$	Electrolyte-phase potential in region k	V	✓	✓	✓
$i_k(x, t)$	Local current density in region k	A m^{-2}	✓	✓	✓
$c_{s,k}(x, r, t)$	Concentration of Li^+ on the intercalation particle of electrode k	mol m^{-3}	✓	-	✓
$\Phi_{s,k}(x, t)$	Solid-phase potential of electrode k	V	✓	-	✓
$j_{n,k}(x, t)$	Pore wall flux of Li^+ on the intercalation particle of electrode k	$\text{mol m}^{-2} \text{s}^{-1}$	✓	-	✓
$\kappa_{0,k}(x, t)$	Ionic conductivity of the electrolyte in region k	S cm^{-1}	✓	✓	✓
$U_k(x, t)$	Open-circuit potential of electrode k	V	✓	-	✓

Table 2: Estimated parameters in Li-Ion Model.

Parameter	Description	Unit	Initial Guess	True Value
			θ_{IG}	θ^*
$D_{s,a}$	Li^+ diffusion coefficient in the solid particle of anode	$\text{m}^2 \text{s}^{-1}$	1.50×10^{-13}	1.00×10^{-13}
$D_{s,c}$	Li^+ diffusion coefficient in the solid particle of cathode	$\text{m}^2 \text{s}^{-1}$	1.13×10^{-10}	7.50×10^{-11}
D	Salt diffusion coefficient in the electrolyte	$\text{m}^2 \text{s}^{-1}$	5.85×10^{-14}	3.90×10^{-14}
k_a	Reaction rate constant in the anode	$\text{m}^{2.5} \text{mol}^{-0.5} \text{s}^{-1}$	3.00×10^{-11}	2.00×10^{-11}
k_c	Reaction rate constant in the cathode	$\text{m}^{2.5} \text{mol}^{-0.5} \text{s}^{-1}$	3.00×10^{-11}	2.00×10^{-11}
p	Bruggman coefficient	-	2.25	1.5
R_f	Film resistance at the anode	Ωm^2	0.135	0.090
t_+	Transport number	-	0.363	0.363

We have performed the following modifications to the model to aid computational performance:

- The local current density i_k with $k = \{a, s, c\}$ is eliminated at the electrodes and the electrolyte by substituting Faraday's equation in Ohm's equation. With this simplification the model reduces to seventeen dependent variables given by $c_{e,a}(x, t)$, $c_{e,s}(x, t)$, $c_{e,c}(x, t)$, $\Phi_{e,a}(x, t)$, $\Phi_{e,s}(x, t)$, $\Phi_{e,c}(x, t)$, $c_{s,a}(x, r, t)$, $c_{s,c}(x, r, t)$, $\Phi_{s,a}(x, t)$, $\Phi_{s,c}(x, t)$, $j_{n,a}(x, t)$, $j_{n,c}(x, t)$, $\kappa_{0,a}(x, t)$, $\kappa_{0,s}(x, t)$, $\kappa_{0,c}(x, t)$, $U_a(x, t)$ and $U_c(x, t)$.
- The three PDEs representing the electrolyte phase concentrations across the three regions (i.e., anode $c_{e,a}(x, t)$, separator $c_{e,s}(x, t)$ and cathode $c_{e,c}(x, t)$) are approximated by a single PDE with the axis dimension spanning $x \in [0, L]$. The new variable is called $c_e(x, t)$. The same simplification is made for the electrolyte phase potentials (i.e., anode $\Phi_{e,a}(x, t)$, separator $\Phi_{e,s}(x, t)$ and cathode $\Phi_{e,c}(x, t)$). The new continuous variable is $\Phi_e(x, t)$. This reduces the system to thirteen dependent variables given by $c_e(x, t)$, $\Phi_e(x, t)$, $c_{s,a}(x, r, t)$, $c_{s,c}(x, r, t)$, $\Phi_{s,a}(x, t)$, $\Phi_{s,c}(x, t)$, $j_{n,a}(x, t)$, $j_{n,c}(x, t)$, $\kappa_{0,a}(x, t)$, $\kappa_{0,s}(x, t)$, $\kappa_{0,c}(x, t)$, $U_a(x, t)$ and $U_c(x, t)$.
- We modify the boundary conditions for the potential of both electrodes and of the electrolyte. Specifically, we set $\Phi_e(0, t) = \Phi_{e,0}$ and $\Phi_{s,c}(\ell_a + \ell_s, t) = \Phi_{s,c,0}$. We also introduce two additional

Table 3: Operating and design variables, constants and fixed parameters in Li-Ion Model.

Variable /Parameter	Description	Unit	Anode ($k = a$)	Separator ($k = s$)	Cathode ($k = c$)
Operating variables					
I	Discharge current (1.0 C)	A m ⁻²		17.5	
T	Temperature	K		298	
Design variables					
$c_e^{(0)}$	Initial electrolyte concentration in region k	mol m ⁻³		2000	
$c_{s,k}^{(0)}$	Initial concentration of Li^+ in electrode k	mol m ⁻³	14870	-	3900
$\Phi_{e,0}$	Electrolyte potential at $x = 0$	V	0	-	-
$\Phi_{s,c,0}$	Electrode potential at $x = \ell_a + \ell_s$	V	-	-	4.2
ℓ_k	Thickness of region k	μ m	100	52	174
ϵ_k	Porosity of region k	-	0.357	1	0.444
$\epsilon_{f,k}$	Volume fraction of fillers in region k	-	0.172	-	0.259
Physical constants					
F	Faraday's constant	C mol ⁻¹		96487	
R	Ideal gas constant	J mol ⁻¹ K ⁻¹		17.5	
Kinetic and transport parameters					
$c_{s,k,max}$	Max. concentration of Li^+ in electrode k	mol m ⁻³	26390	-	22860
$R_{s,k}$	Radius of active material in electrode k	μ m	12.5	-	8.5
σ_k	Electronic conductivity of electrode k	S m ⁻¹	100	-	3.8

equations related to the integral form of Faraday's law (see integral equations in Table 5). The transformations are based on the fact that the current supplied by each portion of the anode and cathode should add up to the total current I .

- We apply L'Hopital's theorem to the Li-ion diffusion equation in the solid active material (derived from Fick's law) to avoid the indeterminate boundary condition at the sphere center ($r = 0$). Consequently, an additional equation is introduced to represent the concentration of Li^+ ions in the solid-phase of the electrodes ($c_{s,a}(x, r, t)$ and $c_{s,c}(x, r, t)$).
- We use a dimensionless model in the axial x and spherical coordinates r . Each region is normalized according to its width. For instance, we define $x^* = x/\ell_a$ and $r^* = r/R_{s,a}$ in the anode.

The complete set of equations of the modified model is presented in Tables 4 and 5. The PDAE system is discretized in the axial and spatial coordinates to obtain a set of DAEs. We obtain consistent initial conditions for this DAE system as follows. The algebraic equations of the discretized system and those of the most interconnected variables are decoupled from the whole model $t = 0$ (i.e., $j_{n,a}(x, t)$, $j_{n,c}(x, t)$, $\Phi_{s,a}(x, t)$, $\Phi_{s,c}(x, t)$ and $\Phi_e(x, t)$). Here, the electrolyte concentration functions for $\kappa_{0,k}(c_e(x, t))$ with $k = \{a, s, c\}$ and $U_k(c_{e,k}(x, t))$ with $k = \{a, c\}$ are also included. We solve these equations by assuming all the concentrations equal to their initial values ($c_e(x, 0) = c_e^{(0)}$, $c_{s,a}(x, r, 0) = c_{s,a}^{(0)}$ and $c_{s,c}(x, r, 0) = c_{s,c}^{(0)}$). With this initial solution of the pore wall flux of Li^+ ions (i.e., $j_{n,a}(x, 0) = j_{n,a}^{(0)}$, $j_{n,c}(x, 0) = j_{n,c}^{(0)}$) and potentials ($\Phi_{s,a}(x, 0) = \Phi_{s,a}^{(0)}$, $\Phi_{s,c}(x, 0) = \Phi_{s,c}^{(0)}$ and $\Phi_e(x, 0) = \Phi_e^{(0)}$) we solve the discretized PDEs for the concentrations ($c_e(x, t)$, $c_{s,a}(x, r, t)$, and $c_{s,c}(x, r, t)$).

Table 4: Governing equations for modified Li-ion PDAE model.

Region	Governing Equation	Boundary Condition I	Boundary Condition II	Initial Condition
Anode	Solid-phase potential: $\Phi_{s,a}(x, t)$ $\sigma_{eff,a} \frac{\partial^2 \Phi_{s,a}(x,t)}{l_a^2 \partial x^2} = F a_a j_{n,a}(x, t)$	$x = 0$ $\Phi_{s,a}(x, t) = 0$	$x = l_a$ $\frac{\partial \Phi_{s,a}(x,t)}{\partial x} = 0$	
	Solid-phase concentration: $c_{s,a}(x, r, t)$ $\frac{\partial c_{s,a}(x,r,t)}{\partial t} = 3 \frac{D_{s,a}}{R_{s,a}^2} \frac{\partial^2 c_{s,a}(x,r,t)}{\partial r^2}$ if $r = 0$ $\frac{\partial c_{s,a}(x,r,t)}{\partial t} = \frac{D_{s,a}}{R_{s,a}^2} \frac{\partial^2 c_{s,a}(x,r,t)}{\partial r^2} + 2 \frac{\partial c_{s,a}(x,r,t)}{r \partial r}$ if $r > 0$	$r = 0$ $\frac{\partial c_{s,a}(x,r,t)}{\partial r} = 0$	$r = R_{s,a}$ $\frac{\partial c_{s,a}(x,r,t)}{\partial r} = -R_{s,a} \frac{j_{n,a}(x,t)}{D_{s,a}}$	$t = 0$ $c_{s,a}(x, r, 0) = c_{s,a}^{(0)}$
	Solid-phase potential: $\Phi_{s,c}(x, t)$ $\sigma_{eff,c} \frac{\partial^2 \Phi_{s,c}(x,t)}{l_c^2 \partial x^2} = F a_c j_{n,c}(x, t)$	$x = l_a + l_s$ $\Phi_{s,c}(x, t) = \Phi_{s,c,0}$	$x = l_a + l_s + l_c$ $\frac{\partial \Phi_{s,c}(x,t)}{\partial x} = -l_c \frac{I}{\sigma_{eff,c}}$	
Cathode	Solid-phase concentration: $c_{s,c}(x, r, t)$ $\frac{\partial c_{s,c}(x,r,t)}{\partial t} = 3 \frac{D_{s,c}}{R_{s,c}^2} \frac{\partial^2 c_{s,c}(x,r,t)}{\partial r^2}$ if $r = 0$ $\frac{\partial c_{s,c}(x,r,t)}{\partial t} = \frac{D_{s,c}}{R_{s,c}^2} \frac{\partial^2 c_{s,c}(x,r,t)}{\partial r^2} + 2 \frac{\partial c_{s,c}(x,r,t)}{r \partial r}$ if $r > 0$	$r = 0$ $\frac{\partial c_{s,c}(x,r,t)}{\partial r} = 0$	$r = R_{s,c}$ $\frac{\partial c_{s,c}(x,r,t)}{\partial r} = -R_{s,c} \frac{j_{n,c}(x,t)}{D_{s,c}}$	$t = 0$ $c_{s,c}(x, r, 0) = c_{s,c}^{(0)}$
	Electrolyte-phase potential: $\Phi_e(x, t)$ $\kappa_{eff} \frac{\partial^2 \Phi_e(x,t)}{l^2 \partial x^2} = \frac{2\kappa_{eff}(x,t)RT}{F} (1 - t_+) \frac{\partial^2 c_e(x,t)}{l^2 \partial x^2} - F a j_n(x, t)$	$x = 0$ $\Phi_e(x, t) = \Phi_{e,0}$	$x = l_a + l_s + l_c$ $\frac{\partial \Phi_e(x,t)}{\partial x} = 0$	
Separator Cathode	Electrolyte-phase concentration: $c_e(x, t)$ $\epsilon \frac{\partial c_e(x,t)}{\partial t} = D_e f \frac{\partial^2 c_e(x,t)}{l^2 \partial x^2} + a(1 - t_+) j_n(x, t)$	$x = 0$ $\frac{\partial c_e(x,t)}{\partial x} = 0$	$x = l_a + l_s + l_c$ $\frac{\partial c_e(x,t)}{\partial x} = 0$	$t = 0$ $c_e(x, 0) = c_e^{(0)}$

Table 5: Auxiliary Equations of modified Li-ion PDAE model.

Region	Auxiliary equation
Anode	$\sigma_{eff,a} = \sigma_a \epsilon_a^p$ $a_a = \frac{3}{R_{s,a}} (1 - \epsilon_a - \epsilon_{f,a})$ $j_{n,a}(x, t) = 2 k_a (c_{s,a}(x, R_{s,a}, t))^{0.5} (c_{e,a}(x, t))^{0.5} (c_{s,a,max} - c_{s,a}(x, R_{s,a}, t))^{0.5} \sinh\left(\frac{0.5F}{RT} (\Phi_{s,a}(x, t) - \Phi_{e,a}(x, t) - U_a(x, t) - F j_{n,a}(x, t) R_f)\right)$ $U_a(x, t) = -0.16 + 1.32 e^{-3 \frac{c_{s,a}(x, R_{s,a}, t)}{c_{s,a,max}}} + 10 e^{-2000 \frac{c_{s,a}(x, R_{s,a}, t)}{c_{s,a,max}}}$ $\int_0^{\ell_a} (F a_a j_{n,a}(x, t) _{\Phi_{s,a}=\Phi_{e,0}}) dx = I$
Cathode	$\sigma_{eff,c} = \sigma_c \epsilon_c^p$ $a_c = \frac{3}{R_{s,c}} (1 - \epsilon_c - \epsilon_{f,c})$ $j_{n,c}(x, t) = 2 k_c c_{s,c}(x, R_{s,c}, t)^{0.5} c_{e,c}(x, t)^{0.5} (c_{s,c,max} - c_{s,c}(x, R_{s,c}, t))^{0.5} \sinh\left(\frac{0.5F}{RT} (\Phi_{s,c}(x, t) - \Phi_{e,c}(x, t) - U_c(x, t))\right)$ $U_c(x, t) = 4.198 + 0.0565 \tanh\left(-14.554 \frac{c_{s,c}(x, r, t) _{r=R_{s,c}}}{c_{s,c,max}} + 8.609\right) - 0.0275 \left(\frac{1}{(0.9984 - \frac{c_{s,c}(x, r, t) _{r=R_{s,c}}}{c_{s,c,max}})^{0.492}} - 1.901 \right) - 0.157 e^{-0.0473 \left(\frac{c_{s,c}(x, r, t) _{r=R_{s,c}}}{c_{s,c,max}} \right)^8} + 0.8102 e^{-40 \left(\frac{c_{s,c}(x, r, t) _{r=R_{s,c}}}{c_{s,c,max}} - 0.133 \right)}$ $\int_{\ell_a+\ell_s}^{\ell_a+\ell_s+\ell_c} (F a_c j_{n,c}(x, t) _{\Phi_{s,c}=\Phi_{s,c,0}}) dx = -I$
Anode/ Separator/ Cathode $k = \{a, s, c\}$	$\Phi_e(x, t) = (\Phi_{e,a}(x, t), \Phi_{e,s}(x, t), \Phi_{e,c}(x, t))$ $c_e(x, t) = (c_{e,a}(x, t), c_{e,s}(x, t), c_{e,c}(x, t))$ $j_n(x, t) = (j_{n,a}(x, t), 0, j_{n,c}(x, t))$ $\kappa_{eff}(x, t) = (\kappa_{eff,a}(x, t), \kappa_{eff,s}(x, t), \kappa_{eff,c}(x, t))$ $\kappa_{eff,k}(x, t) = (1 \times 10^2 \kappa_{0,k}(x, t)) \epsilon_k^p$ $\kappa_{0,k}(x, t) = 1.0793 \times 10^{-4} + 6.7461 \times 10^{-3} (1 \times 10^{-3} c_{e,k}(x, t)) - 5.2245 \times 10^{-3} (1 \times 10^{-3} c_{e,k}(x, t))^2 + 1.3605 \times 10^{-3} (1 \times 10^{-3} c_{e,k}(x, t))^3 - 1.1724 \times 10^{-4} (1 \times 10^{-3} c_{e,k}(x, t))^4$ $D_{eff} = (D_{eff,a}, D_{eff,s}, D_{eff,c})$ $D_{eff,k} = D \epsilon_k^p$ $\epsilon = [\epsilon_a, \epsilon_s, \epsilon_c]$ $l = [l_a, l_s, l_c]$ $a = [a_a, 0, a_c]$

4 Case Study

The PDAE system is discretized by the method of lines in the axial and radial dimensions. The resulting DAE system contains 561 equations. The differential and algebraic state variable vectors defined in (2.1) are given by $x = (c_e, c_{s,a}, c_{s,c})$ and $z = (\Phi_e, \Phi_{s,a}, \Phi_{s,c}, j_{n,a}, j_{n,c}, \kappa_{0,a}, \kappa_{0,s}, \kappa_{0,c}, U_a, U_c)$, respectively (states are assumed to be discretized). The parameter vector is $\theta = (D, D_{s,a}, D_{s,c}, k_a, k_c, p, R_f, t_+)$. We consider the cell voltage $V_{cell}(t)$ and the electrolyte concentration in the separator core $c_e(\ell_a + \ell_s/2, t)$ as the predicted response variable; we thus have $y = (V_{cell}(t), c_e(\ell_a + \ell_s/2, t))$. The cell voltage $V_{cell}(t)$ is computed using the solid-phase potential on the right-hand side of the cathode $\Phi_{s,c}(\ell_a + \ell_s + \ell_c, t)$ and on the left-hand side of the anode $\Phi_{s,a}(0, t)$ as,

$$V_{cell}(t) = \Phi_{s,c}(\ell_a + \ell_s + \ell_c, t) - \Phi_{s,a}(0, t) \quad (4.17)$$

We also consider constant discharge current rates I (galvanostatic process) as the input or controls $u = I$. The change of $V_{cell}(t)$ for a discharge rate I is known as the *voltage discharge curve*. The cell voltage $V_{cell}(t)$ and the electrolyte concentration in the separator core $c_e(\ell_a + \ell_s/2, t)$ are assumed to be measured at 100 (equally spaced) time points $\bar{Y} = (V_{cell}(t_k), c_e(\ell_a + \ell_s/2, t_k))$, for $t_k \in \mathcal{T} = \{1, \dots, 100\}$. The discharge curve at I_1 is shown in Figure 2.

To investigate if information provided by discharge curves is sufficient to reliably estimate key parameters of interest we analyze two different cases that we refer to as Case 1 and Case 2. Case 1 is analyzed in detail to discuss the different techniques of our framework while Case 2 is presented in summarized form. We use a third case (Case 3) to demonstrate that the use of electrolyte concentration information dramatically improves identifiability. We summarize the three cases as follows:

- Case 1 (base case): we consider one experiment that only uses discharge curve information (we set I_1 as the standard discharge rate). The only observable variable is assumed to be $V_{cell}(\cdot)$.
- Case 2: we consider the effect of progressively adding experiments with discharge curve information (we set I_i , $i = 2, \dots, 6$). The only observable variable is assumed to be $V_{cell}(\cdot)$.
- Case 3: we consider the effect of progressively adding experiments with discharge curve information and include the electrolyte concentration in the middle of the separator $c_e(\ell_a + \ell_s/2, \cdot)$ as observable variable (we set I_i , $i = 1, \dots, 4$). The observable variables are $V_{cell}(\cdot)$ and $c_e(\cdot)|_{x=\ell_a+\ell_s/2}$.

We apply the sensitivity-based and Monte Carlo strategies of Section 2.2 to analyze parameters. The results of Case 1 (base case), 2 and 3 are presented in Sections 4.1, 4.2, and 4.3, respectively. In Table 2 we display the true parameter vector θ^* taken from [12] and the initial guess vector θ_{IG} . In all cases, the experimental data \bar{Y} is virtually generated by perturbing the model solution $Y(u, \theta^*)$ at u and θ^* under measurement error samples drawn from a normal distribution with mean zero and variance $\sigma_y^2 = 1 \times 10^{-4}$. In other words, $\bar{Y} = Y(u, \theta^*) + \epsilon$ with $\epsilon \sim \mathcal{N}(0, \sigma_y^2 I)$. To aid numerical stability, the response variables and parameters are normalized. In Figure 2 we display the discharge curves for Cases 1 and 2. The discharge rates I are expressed relative to the base current $C = 17.5 A/m^2$. We thus have that $I_1 = 1C$ (base discharge), $I_2 = 2C$, $I_3 = 3C$, $I_4 = 4C$ (fast discharge), and $I_5 = 0.5C$ and $I_6 = 0.1C$ (slow discharge). We assume a cut-off voltage of 2.8V.

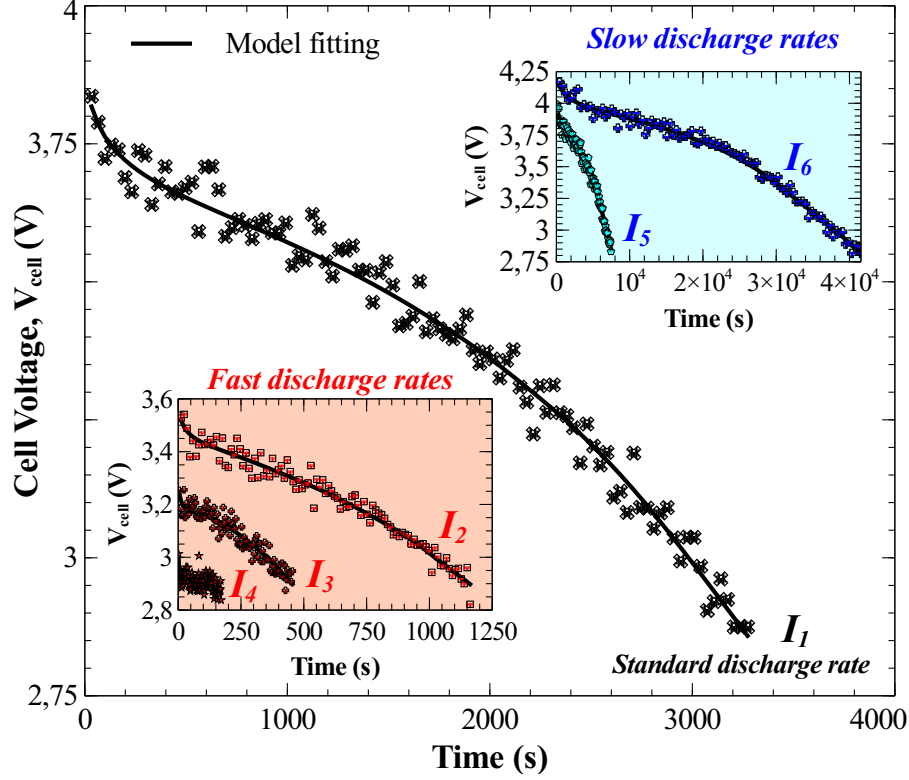


Figure 2: Discharge curves for base ($I_1 = 1C$), fast ($I_2 = 2C$, $I_3 = 3C$, $I_4 = 4C$), and slow rates ($I_5 = 0.5C$ and $I_6 = 0.1C$). Markers are experimental data and solid lines are model predictions after parameter estimation (at estimator $\hat{\theta}$).

4.1 Case 1: Single Discharge Curve.

4.1.1 Sensitivity Method

The results of the sensitivity method discussed in Section 2.2.1 are summarized in Table 6. We present the estimate $\hat{\theta}$ and their variances $\sigma_{j_j}^2$ (diagonal elements of C computed from (2.8)). The estimator accuracy is measured in terms of the squared bias $\beta(\hat{\theta})^2$ computed from (2.15) and MSE computed from (2.16). The model predictions at $\hat{\theta}$ are shown in Figure 2.

Estimator Analysis. Despite the good fitting exhibited in Figure 2, the estimated parameters have large variances if only one discharge curve (I_1) is used as experimental data. The most precise parameter is the Li^+ ion diffusion coefficient in the solid particle of the anode $D_{s,a}$ with a variance of 3.56×10^{-2} and the worst is the reaction rate constant in the anode k_a with variance of 4.40×10^{15} . The precision of each parameter in terms of the length of their confidence intervals presented in (2.14) is shown in Table 7. The lengths are computed as percentages relative to $\bar{\theta}^*$.

We now quantify the estimator accuracy in terms of its bias. The film resistance at the anode R_f presents a bias of $\beta(\hat{\theta})^2 = 4.65 \times 10^{-3}$ which is equivalent to a relative bias of $\beta(\hat{\theta})/\bar{\theta}^* = 10\%$. The parameter k_a exhibits the largest bias ($\beta(\hat{\theta})^2 = 1.56 \times 10^7$) equivalent to a relative bias of $5.92 \times 10^5\%$. The overall performance metrics of this parameter estimator are 4.40×10^{15} for precision (related to

Table 6: Case 1 for Sensitivity method.

Parameter	True $\hat{\theta}^*$	Estimated $\hat{\theta}$	Estimator Performance			Identifiability analysis (Parameter Ranking)		
			Precision	Accuracy		Variance Method	SVD Method	QRP Method
			Variance σ^2	Bias $\beta(\hat{\theta})^2$	MSE			
$D_{s,a}$	6.67×10^{-1}	2.54×10^{-1}	3.56×10^{-2}	1.70×10^{-1}	2.06×10^{-1}	(1)*	(1)	(2)*
$D_{s,c}$	6.67×10^{-1}	9.13×10^{-1}	$5.79 \times 10^{+2}$	6.07×10^{-2}	$5.79 \times 10^{+2}$	(7)	(7)	(7)
D	6.67×10^{-1}	$1.32 \times 10^{+0}$	$1.48 \times 10^{+1}$	4.25×10^{-1}	$1.52 \times 10^{+1}$	(5)	(5)	(5)
k_a	6.67×10^{-1}	$3.95 \times 10^{+3}$	$4.40 \times 10^{+15}$	$1.56 \times 10^{+7}$	$4.40 \times 10^{+15}$	(8)	(8)	(8)
k_c	6.67×10^{-1}	7.40×10^{-1}	$3.84 \times 10^{+1}$	5.45×10^{-3}	$3.85 \times 10^{+1}$	(6)	(6)	(6)
p	6.67×10^{-1}	7.93×10^{-1}	$1.55 \times 10^{+0}$	1.59×10^{-2}	$1.56 \times 10^{+0}$	(2)	(2)	(1)*
R_f	6.67×10^{-1}	5.98×10^{-1}	$6.13 \times 10^{+0}$	4.65×10^{-3}	$6.13 \times 10^{+0}$	(3)	(4)	(4)
t_+	$1.00 \times 10^{+0}$	2.92×10^{-1}	$9.83 \times 10^{+0}$	5.01×10^{-1}	$1.03 \times 10^{+1}$	(4)	(3)	(3)*
Identifiable Subset Dimension						1	0	3

Table 7: Case 1, 2, and 3: Confidence interval lengths for Sensitivity and Monte Carlo methods. Lengths are expressed as percentages relative to the true parameter.

Parameter	Sensitivity Method			Monte Carlo Method				
	Case 1	Case 2		Case 1	Case 2		Case 3	
	SC_1	SC_4	SC_6	SC_1	SC_4	SC_6	SC_1	SC_4
$D_{s,a}$	$1.1 \times 10^2\%$	$5.3 \times 10^1\%$	$6.1 \times 10^1\%$	$6.0 \times 10^3\%$	$1.9 \times 10^2\%$	$1.6 \times 10^2\%$	$4.6 \times 10^2\%$	$5.8 \times 10^1\%$
$D_{s,c}$	$1.4 \times 10^4\%$	$5.5 \times 10^2\%$	$3.6 \times 10^2\%$	$8.7 \times 10^5\%$	$1.3 \times 10^5\%$	$9.3 \times 10^3\%$	$2.4 \times 10^5\%$	$1.4 \times 10^2\%$
D	$2.3 \times 10^3\%$	$2.3 \times 10^2\%$	$2.2 \times 10^2\%$	$8.4 \times 10^4\%$	$1.7 \times 10^2\%$	$8.2 \times 10^1\%$	$6.0 \times 10^1\%$	$2.4 \times 10^1\%$
k_a	$3.9 \times 10^{10}\%$	$2.2 \times 10^2\%$	$1.5 \times 10^2\%$	$1.4 \times 10^6\%$	$1.4 \times 10^6\%$	$9.3 \times 10^3\%$	$4.4 \times 10^6\%$	$8.7 \times 10^5\%$
k_c	$3.7 \times 10^3\%$	$9.1 \times 10^2\%$	$9.0 \times 10^2\%$	$6.3 \times 10^5\%$	$5.3 \times 10^2\%$	$5.1 \times 10^2\%$	$1.1 \times 10^2\%$	$8.4 \times 10^1\%$
p	$7.4 \times 10^2\%$	$8.3 \times 10^1\%$	$7.1 \times 10^1\%$	$1.4 \times 10^2\%$	$4.9 \times 10^1\%$	$3.7 \times 10^1\%$	$2.2 \times 10^1\%$	$8.0 \times 10^0\%$
R_f	$1.5 \times 10^3\%$	$6.5 \times 10^1\%$	$6.4 \times 10^1\%$	$1.4 \times 10^2\%$	$3.7 \times 10^1\%$	$2.9 \times 10^1\%$	$1.4 \times 10^2\%$	$1.2 \times 10^1\%$
t_+	$1.2 \times 10^3\%$	$5.8 \times 10^1\%$	$4.8 \times 10^1\%$	$2.4 \times 10^2\%$	$4.5 \times 10^1\%$	$3.8 \times 10^1\%$	$4.2 \times 10^1\%$	$1.0 \times 10^1\%$

$\text{Tr}[C]$) and 1.56×10^7 for bias (as the squared norm of $\beta(\hat{\theta})$). With these results we observe that the estimator for Case 1 is highly unstable.

Ill-Conditioning Analysis. We now explore structural issues by applying the procedures of Section 2.4.1. This is based on the singular value analysis of the scaled sensitivity matrix S evaluated at the parameter estimate $\hat{\theta}$. The singular values of S vary from $\varsigma_1 = 9.1087 \times 10^1$ to $\varsigma_8 = 1.5074 \times 10^{-8}$. The spectrum of the singular values SVs is the black-solid line with markers in Figure 3 (left panel). The condition number and the collinearity index are $\kappa = 6.0428 \times 10^9$ and $\gamma = 6.6341 \times 10^7$, respectively.

On the left-hand side of Figure 3 we present lower bounds with respect to the condition number and the collinearity index, ϵ_κ and ϵ_γ , respectively for Case 1. These values are computed by using the predefined empirical upper bounds $\kappa^{max} = 1000$ [21, 30, 29] and $\gamma^{max} = 15\sigma_y$ [6, 30, 29]. The bound γ^{max} is scaled by the measurement standard deviation σ_y because we consider the scaled sensitivity matrix $S = \Sigma_y^{-1} \nabla_{\theta} Y$. We set $\epsilon = \epsilon_\gamma = 6.67 \times 10^0$ as the lowest bound on the SVs to select the well-conditioned singular values. For Case 1, only three singular values pass this test, which implies that S has a numerical rank of three ($r_\epsilon = 3$) and we have five ill-conditioned singular values.

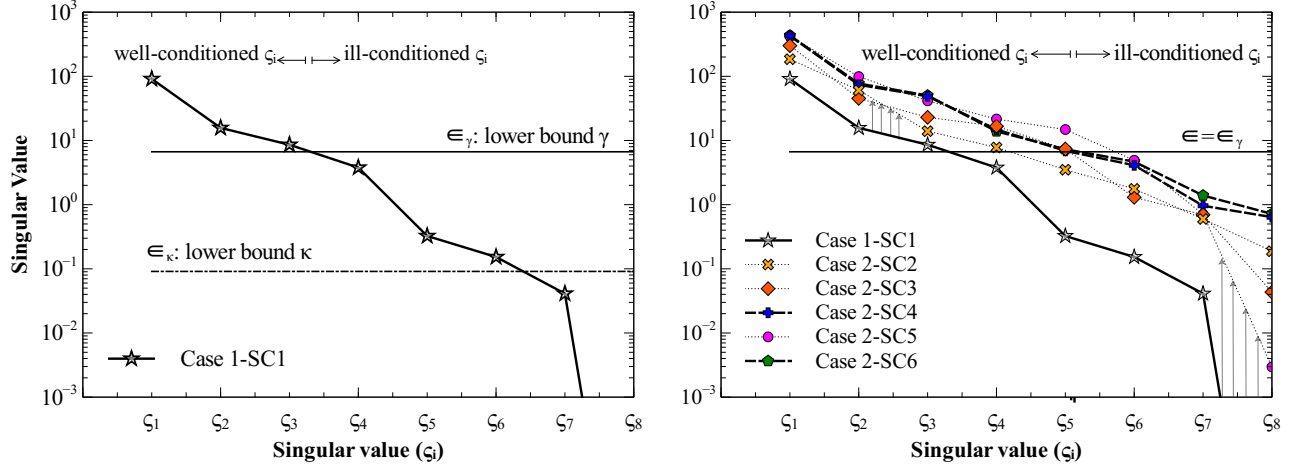


Figure 3: Singular value spectra. Left panel is Case 1 (single discharge curve) and right panel is Case 2 (multiple discharge curves).

Identifiability Analysis. We now apply the three different identifiability analysis methods (variance, SVD, and QRP) described in Section 2.4.2. We show the identifiable ranking list obtained for each method in Table 6. The numbers in parenthesis indicate the position of each parameter in the ranking and the stars indicate the identifiable parameters according to each method.

- *Variance Method:* under to this method the most identifiable parameter is $D_{s,a}$ (smallest variance of $\sigma_{D_{s,a}}^2 = 3.56 \times 10^{-2}$), and the less identifiable parameter is k_a (largest variance of $\sigma_{k_a}^2 = 4.40 \times 10^{15}$). If we use a variance threshold of $\rho = 1.5 \times 10^{-1}$ [41] we have that only one parameter is considered identifiable.
- *SVD Method:* under this method we find a similar ranking. In Figure 4 we present the contribution of each singular value to the variance of each parameter. We highlight the strong influence of the ill-conditioned singular values (i.e., ζ_i for $i = 4, \dots, 8$) on the variance. These are responsible for the large variances observed in Table 6. We also see that the last two parameters in the identifiable ranking list ($D_{s,c}$ and k_a) are fully influenced by the smallest singular values ζ_7 and ζ_8 , respectively (proportions of 100%). The most identifiable parameter $D_{s,a}$ exhibits the smallest impact from the ill-conditioned singular values. The proportion, however, is still significant (79.5%). In fact, if we use a proportion threshold $\pi^{max} = 50\%$ [4] to select the identifiable parameters, this would indicate that we cannot classify $D_{s,a}$ as an identifiable parameter. Accordingly, *all parameters would be considered unidentifiable*. In Table 6 we thus present a parameter subset dimension equal to zero. From Figure 4 it also becomes evident that the smallest singular values ζ_i for $i = 4, \dots, 8$ simultaneously affect many parameters. This is an indication of linear dependence.
- *QR Method:* under this method we find that the parameter with the most effect on the outputs is the Bruggman coefficient p . Consequently, in Table 6 we put this parameter on the first place

of the ranking. The reaction rate constant in the anode k_a is the last in the ranking. This means that, after all orthogonal projections, this parameter has the smallest effect on the measured variables. In order to select the number of the identifiable parameters, we use $r_\epsilon = 3$ such that the identifiable parameter subset dimension is 3. Under this threshold, we obtain that parameters p , $D_{s,a}$ and t_+ are identifiable.

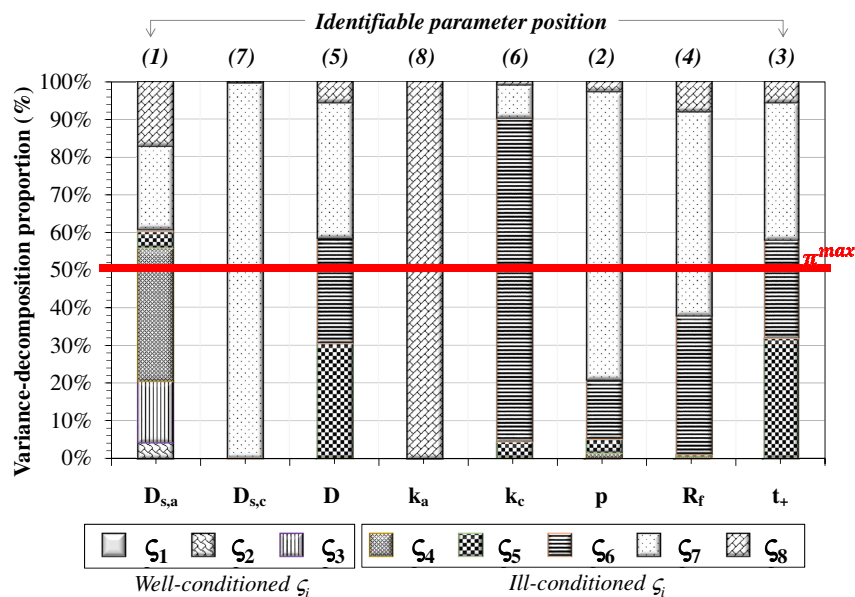


Figure 4: Case 1: Variance decomposition for SVD identifiability method of Section 2.4.2.

From previous results we can establish several conclusions. First, the three methods indicate that we cannot identify the whole parameter vector using one discharge curve. This is because the discharge signal $u = I_1$ does not excite enough the system and this is manifested as ill-conditioning of the sensitivity matrix S . This is reinforced by Figure 5, where we present the sensitivity time profiles of the voltage to the different parameters. As can be seen, the measured variable V_{cell} is not significantly excited by several parameters (several time profiles are flat and close to zero). We thus find insensitive parameters (e.g., k_a , $D_{s,c}$ and k_c) which can take any value in a broad space without affecting the output. We can also conclude that parameter variability and identifiability issues are closely related to the ill-conditioning of the sensitivity matrix S . Accordingly, any improvement in the ill-conditioning of S will have a beneficial impact in parameter variances, confidence intervals and identifiability. This can be achieved by providing alternative discharge signals that more properly excite the system.

4.1.2 Monte Carlo Method

The sensitivity method provides several indications of poor identifiability. In this section, we use the Monte Carlo method described in Section 2.2.2 to validate these observations. We use $L = 200$

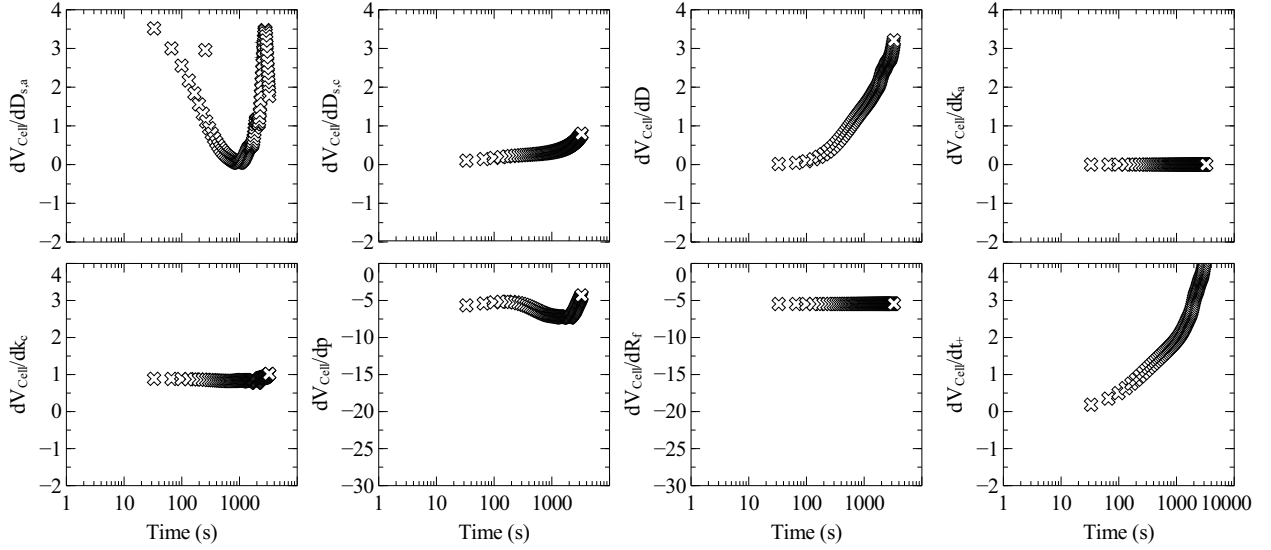


Figure 5: Sensitivity time profiles of cell voltage with respect to parameters $dV_{cell}(t)/d\theta$ at nominal discharge rate I_1 for Case 1.

replications and use the measurement variances $\sigma_y^2 = 1 \times 10^{-4}$ to obtain the data sets \bar{Y}_j . The results are summarized in Table 8. We present the empirical mean $\hat{\theta}$ and the parameter variance σ_{kk}^2 as the diagonal elements of the approximate matrix C . We also present the accuracy performance in terms of the squared bias $\beta(\hat{\theta})^2$ and the MSE. The marginal probability density function (*pdf*) for each parameter are displayed in Figure 6.

Table 8: Case 1: Summary of results for Monte Carlo.

Parameter θ	True $\bar{\theta}^*$	Mean $\hat{\theta}$	Estimator Performance			Identifiability Analysis (Parameter Ranking)
			Precision	Accuracy		
			Variance σ^2	Bias $\beta(\hat{\theta})^2$	MSE	Variance Method
$D_{s,a}$	6.67×10^{-1}	$2.14 \times 10^{+0}$	$1.01 \times 10^{+2}$	$2.16 \times 10^{+0}$	$1.03 \times 10^{+2}$	(4)
$D_{s,c}$	6.67×10^{-1}	$2.24 \times 10^{+2}$	$2.12 \times 10^{+6}$	$5.00 \times 10^{+4}$	$2.17 \times 10^{+6}$	(7)
D	6.67×10^{-1}	$1.24 \times 10^{+1}$	$1.98 \times 10^{+4}$	$1.38 \times 10^{+2}$	$1.99 \times 10^{+4}$	(5)
k_a	6.67×10^{-1}	$6.91 \times 10^{+2}$	$5.42 \times 10^{+6}$	$4.76 \times 10^{+5}$	$4.40 \times 10^{+6}$	(8)
k_c	6.67×10^{-1}	$1.04 \times 10^{+2}$	$1.13 \times 10^{+6}$	$1.07 \times 10^{+4}$	$1.14 \times 10^{+6}$	(6)
p	6.67×10^{-1}	6.97×10^{-1}	5.77×10^{-2}	9.48×10^{-4}	5.86×10^{-2}	(2)*
R_f	6.67×10^{-1}	6.30×10^{-1}	5.55×10^{-2}	1.37×10^{-3}	5.69×10^{-2}	(1)*
t_+	$1.00 \times 10^{+0}$	8.92×10^{-1}	3.74×10^{-1}	1.17×10^{-2}	3.86×10^{-1}	(3)
Performance metric			8.68×10^6	5.37×10^5	9.22×10^6	—
Identifiable Subset Dimension						2

Estimator Analysis. From Table 8 we observe that variances do not match those obtained with the sensitivity method presented in Table 6. This provides evidence that the variances obtained from the Fisher-information matrix are badly approximated. From Table 8 we also see that parameters $D_{s,a}$, $D_{s,c}$, D , k_a and k_c have large variances while parameters p , R_f and t_+ have small ones. This becomes more evident when observing the relative confidence interval lengths presented in Table

7. According to the Monte Carlo method, the most precise parameters are the film resistance at the anode R_f ($\sigma_{R_f}^2 = 5.55 \times 10^{-2}$) and the Bruggman coefficient p ($\sigma_p^2 = 5.77 \times 10^{-2}$). The relative lengths of the confidence intervals for R_f and p , however, are quite large (140% and 143%, respectively). The most uncertain parameter is k_a with a variance of $\sigma_{k_a}^2 = 5.42 \times 10^6$ and a relative length of the confidence interval of $1.38 \times 10^6\%$.

In terms of estimator accuracy, we see that the mean $\hat{\theta}$ presents a deviation from $\bar{\theta}^*$ for parameters $D_{s,a}$, $D_{s,c}$, D and k_c larger than that exhibited by the parameter estimate $\hat{\theta}$ obtained with the sensitivity method and presented in Table 6. This is a reflection of the instability of the parameters. Parameter k_a is the most biased parameter obtained by Monte Carlo. The most precise parameters p , R_f and t_+ are also the least biased parameters. *This ranking is very close to that obtained with the variance, SVD, and QRP methods of the sensitivity setting.*

From Figure 6 we can clearly observe that only parameters p , R_f and t_+ are identifiable and their distribution are close to normal. With these results we confirm that the parameter estimator obtained in Case 1 is unstable.

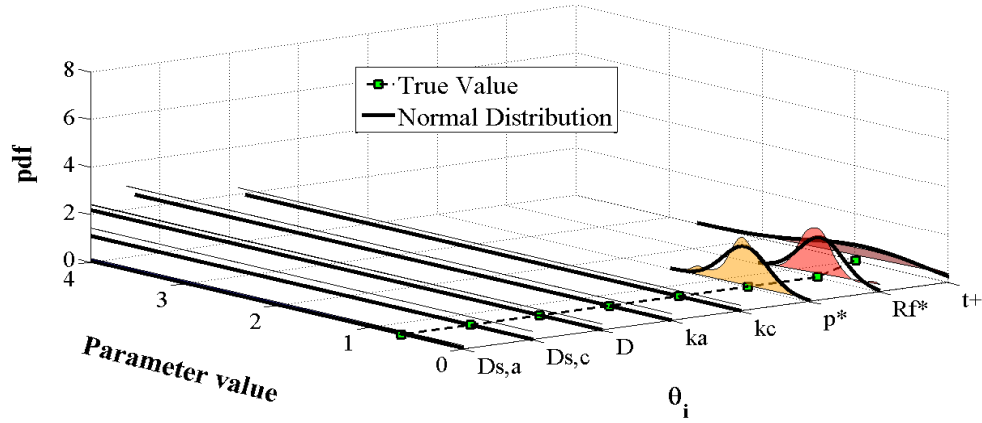


Figure 6: Case 1: Marginal pdfs obtained from Monte Carlo. Solid-black lines and filled regions represent the normal and the non-parametric distributions of each estimator, respectively. Parameters with a star are nominated as identifiable.

Identifiability Analysis. We now apply the variance method of Section 2.4.2 to analyze identifiability under Monte Carlo. Under the variance threshold $\rho = 1.5 \times 10^{-1}$ we find two identifiable parameters, R_f and p . We thus have a identifiable parameter subset dimension equal two, as indicated in Table 8. From this table we also see that the most identifiable parameter is R_f with variance $\sigma_{R_f}^2 = 5.55 \times 10^{-2}$ and the less identifiable parameter is k_a with variance $\sigma_{k_a}^2 = 5.42 \times 10^6$. This is partially consistent with the identifiability results of the sensitivity method.

4.2 Case 2: Multiple Discharge Curves.

From Case 1 we can conclude that only a very small parameter subset is identifiable. In particular, our analysis indicates that parameters R_f , p and t_+ are the only identifiable parameters. Their variances, however, are large. We now analyze the effect of incorporating additional discharge curves. We progressively add new curves obtained at different discharge rates ($I_2 = 2I_1, I_3 = 3I_1, I_4 = 4I_1, I_5 = 0.5I_1$ and $I_6 = 0.1I_1$). The first scenario (denoted as SC_1) uses signal $u_1 = I_1$ and data $\bar{Y}_1 = V_{cell}^1(t_k)$ (this corresponds to Case 1). Scenario SC_2 uses the signal vector $u_2 = (I_1, I_2)$ and data $\bar{Y}_2 = (V_{cell}^1(t_k), V_{cell}^2(t_k))$ and we continue until scenario SC_6 with signal vector $u_6 = (I_1, I_2, \dots, I_6)$ and data $\bar{Y}_6 = (V_{cell}^1(t_k), V_{cell}^2(t_k), \dots, V_{cell}^6(t_k))$.

4.2.1 Sensitivity Method.

We conduct estimation for each scenario SC_1, \dots, SC_6 to obtain the estimates $\hat{\theta}_\xi$, the model prediction vector Y_ξ and its corresponding scaled sensitivity matrix S_ξ . We then analyze the estimator performance for each scenario based on its average estimated covariance matrix C_ξ , confidence intervals, and bias $\beta(\hat{\theta}_\xi)$.

Estimator Analysis. In Table 7 we show the confidence interval lengths in relative terms. We clearly see that the addition of experimental information reduces the confidence levels. The main reduction is observed when four experiments (SC_4) are used. Interestingly, considering two additional experiments (SC_6) only provides a slight improvement over SC_4 . Moreover, despite the reduction in parameter variance over Case 1, we observe that the parameters still have large uncertainties. For instance, for scenario SC_6 , we have that D , $D_{s,c}$ and k_c have interval lengths of 216%, 365% and 902%, respectively.

Considering the large parameter variability we can conclude that information from discharge curves does not seem sufficient to completely identify the parameter vector. *These results also seem to indicate that slow discharge rates I_5, I_6 are not informative.* We corroborated this last observation by analyzing the sensitivity profiles for different rates. In Figure 7 we present the sensitivity profiles for the cell voltage V_{cell} to the parameters for the discharge rates I_1 (standard discharge), I_4 (fast discharge), and I_6 (slow discharge). We observe that the slow discharge rate I_6 provides significantly less excitation compared to I_1 and I_4 . In addition, it is interesting to observe that the *fast discharge rate I_4 induces richer dynamic behavior* (this is particularly evident from the profiles of the Bruggman coefficient and of the diffusion coefficients).

Ill-Conditioning Analysis. We now evaluate changes in ill-conditioning as we add discharge curves. The results are presented in the right panel of Figure 3. We can observe the lifting in the singular value spectrum with each scenario. This lifting is accompanied by a reduction in the spectrum slope (related to the condition number κ) and an increase in the smallest singular value ς_8 (related to the collinearity index γ). In particular, we have condition numbers for SC_4 and SC_6 of 6.668×10^2 and 6.024×10^2 , respectively and collinearity indexes of 1.564×10^0 and 1.395×10^0 . The spectra and the ill-conditioning metrics (κ and γ) demonstrate a significant improvement in the ill-conditioning from

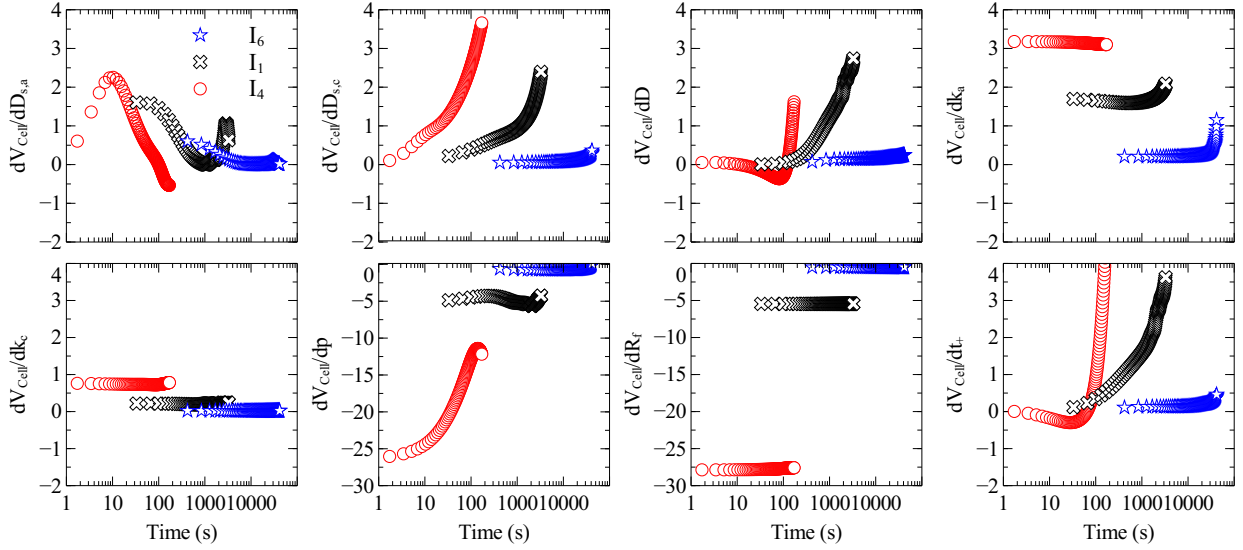


Figure 7: Sensitivity time profiles of cell voltage with respect to parameters $dV_{cell}(t)/d\theta$ at slow I_6 , nominal I_1 , and fast I_4 discharge rates for scenario Case 2- SC_6 .

SC_1 to SC_4 but just a slight improvement of SC_6 with respect to SC_4 . In Figure 3 we also see that the number of well-conditioned singular values is not the full length of the parameter vector. In other words, matrix S has a rank equal to five only ($r_\epsilon=5$).

Identifiability Analysis. In Table 9 we present the subset dimension of the identifiable parameters after applying the three methods of Section 2.4.2. We use the same thresholds of Section 2.3.1 for Case 1. The variance method selects two and six parameters as identifiable for scenarios SC_2 and SC_6 , respectively. This is the result of the progressive reduction of the parameter variance. For SC_4 and SC_6 the identifiable parameters are $D_{s,a}$, k_c , p , R_f and t_+ . Parameters $D_{s,c}$ and k_a remain unidentifiable in all scenarios. The QRP method only selects 5 parameters as identifiable for scenario SC_6 while the SVD method only selects one.

Table 9: Case 2: Summary of results for Sensitivity and Monte Carlo methods.

SC_ξ	New I_ξ	Input action u_ξ	Experimental data Y_ξ^m	Identifiable Subset Dimension			
				Sensitivity Method			Monte Carlo
				Variance	SVD	QR	Method
				Method	Method	Method	Variance Method
1	$1.0 C = 17.5$	$[I_1]$	$[V_{cell}^1]$	1	0	3	2
2	$2.0 C = 35.0$	$[I_1, I_2]$	$[V_{cell}^1, V_{cell}^2]$	2	1	4	3
3	$3.0 C = 52.5$	$[I_1, I_2, I_3]$	$[V_{cell}^1, V_{cell}^2, V_{cell}^3]$	3	1	5	4
4	$4.0 C = 70.0$	$[I_1, I_2, I_3, I_4]$	$[V_{cell}^1, V_{cell}^2, V_{cell}^3, V_{cell}^4]$	5	1	5	5
5	$0.5 C = 8.75$	$[I_1, I_2, I_3, I_4, I_5]$	$[V_{cell}^1, V_{cell}^2, V_{cell}^3, V_{cell}^4, V_{cell}^5]$	6	1	5	5
6	$0.1 C = 1.75$	$[I_1, I_2, I_3, I_4, I_5, I_6]$	$[V_{cell}^1, V_{cell}^2, V_{cell}^3, V_{cell}^4, V_{cell}^5, V_{cell}^6]$	6	1	5	5

4.2.2 Monte Carlo Method.

The variances obtained with Monte Carlo are again several orders of magnitude different than those estimated with the sensitivity method. This is illustrated in Table 7. We can also observe that, because ill-conditioning is improved as we add experimental information, the qualitative behavior of both methods becomes similar. From Table 7 we confirm that the most precise parameters predicted by Monte Carlo are p , R_f and t_+ and a total of five parameters are considered identifiable for SC_4 , SC_5 , and SC_6 . This is consistent with the variance and QRP methods under the sensitivity setting. This again suggests that the sensitivity method can qualitatively diagnose variance behavior. Parameters $D_{s,c}$, k_a and k_c remain with large variance and are unidentifiable.

In Figure 8 we present the marginal probability density functions (pdfs) for scenarios SC_4 and SC_6 . By comparing these pdfs with the pdfs of SC_1 (Case 1) in Figure 6 we clearly see an improvement in the stability of the estimates. From Figure 8 we observe that there is no noticeable difference in the pdfs of scenarios SC_4 and SC_6 for the most precise parameters p , R_f and t_+ . This indicates that, even if the spectrum of singular values does not improve from SC_4 to SC_6 (as suggested by the sensitivity method), there is additional information provided by the discharge rates I_5 and I_6 . This information, however, is still insufficient to determine the rest of the parameters (particularly k_a , k_c , and $D_{s,c}$) which still present large variances.

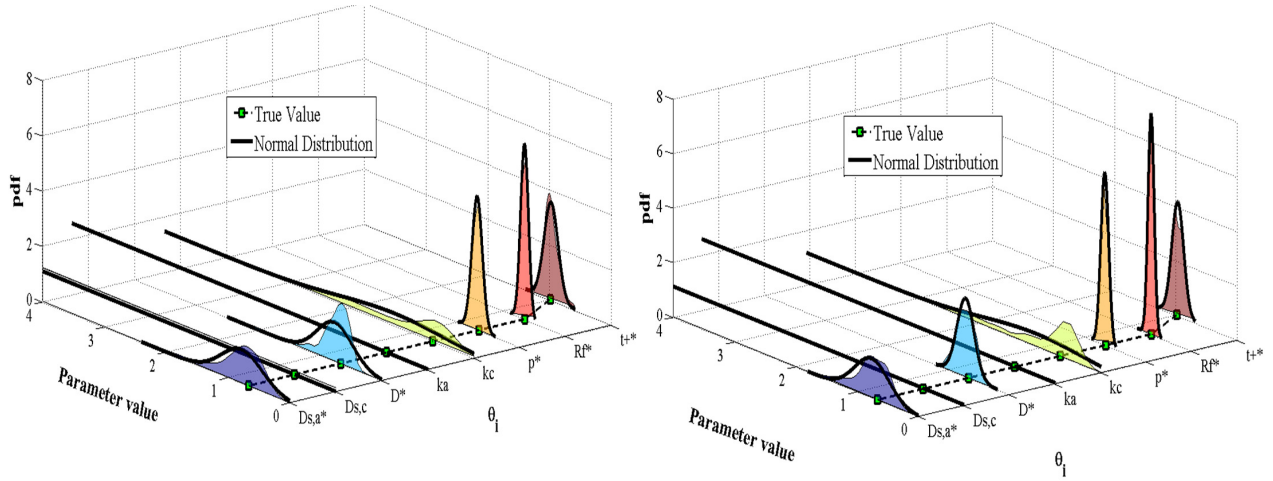


Figure 8: Case 2: Marginal pdfs for parameters obtained with Monte Carlo analysis for scenarios Case 2- SC_4 (left) and Case 2- SC_6 (right).

4.3 Case 3: Discharge curves and electrolyte concentration profile.

In Case 3 we consider two observable variables: $V_{cell}(t)$ and the electrolyte concentration in the middle of the separator $c_e(x, t)|_{x=\ell_a+\ell_s/2}$. We consider scenarios SC_1 , SC_2 , SC_3 , and SC_4 that progressively consider the addition of new experimental information but this time each experiment measures the two outputs. Accordingly, we obtain SC_1 and SC_4 by collecting the experiments at $u_1 = I_1$ and $u_4 = (I_1, \dots, I_4)$, respectively. For consistency, we use the same discharge rates of Case 1 and Case 2.

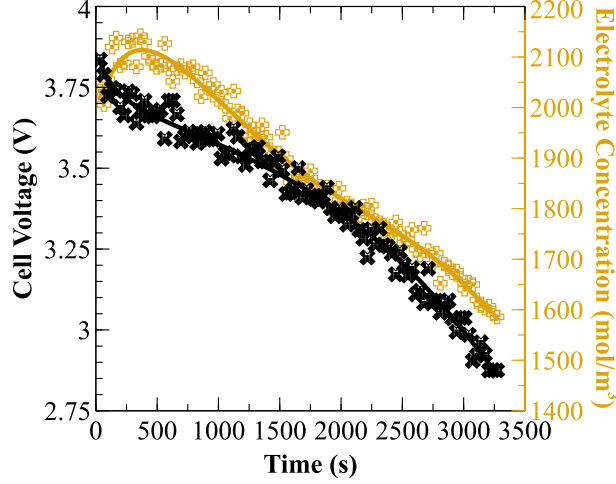


Figure 9: Case 3: Voltage and electrolyte concentration profile at separator for scenario Case 3- SC_1 .

In Figure 9, we display model fitting for both variables after solving the parameter estimation for SC_1 . We highlight the nonlinear response of the concentration profile. In Figure 10 we display the singular value spectra for all considered scenarios. We found a considerable large lift in the spectrum even when only one experiment is used (Case 3- SC_1 compared to Case 1). The form of the new spectrum defines five singular values as well-conditioned compared to three in Case 1. A small singular value of $\varsigma_8 = 9.6113 \times 10^{-9}$, however, is still observed for Case 3- SC_1 . This small singular value makes the condition number large ($\kappa = 6.2796 \times 10^{10}$) and the collinearity index large as well ($\gamma = 1.0404 \times 10^8$). When more experiments are added (Case 3- SC_2 to Case 3- SC_4) the conditioning becomes better with an extra lifting in the spectra and larger values for ς_8 . In Case 3- SC_4 we observe seven well-conditioned singular values compared to the five in Case 2- SC_4 . The effect of adding electrolyte concentration information is thus highly beneficial from an ill-conditioning stand-point.

In Figures 11 and 12 we further illustrate that the improvement in the ill-conditioning is associated with the information supplied by the new observable variable. *By comparing the figures we see that the cell voltage is excited in similar ways for currents I_1 and I_4 while this is not the case for the electrolyte concentration. In particular, the electrolyte concentration presents rich and different dynamic responses at fast and slow rates which aids the identification of parameters.* From Figure 12 we also observe that the electrolyte concentration at the separator core $c_e(\ell_a + \ell_s/2, t)$ is highly excited by parameters D, p and t_+ . Parameters $D_{s,c}$ and k_c also provide more excitation in comparison with Cases 1 and 2 (we recall that $D_{s,c}$ and k_c remain unidentifiable in Case 2).

We further validate our observations for Case 3 using Monte Carlo. In Table 7 we present confidence interval lengths and in Figure 13 we present the pdfs for each parameter for scenarios SC_1 and SC_4 . We observe an important reduction in the confidence intervals compared to Case 2 presented in Table 7. In particular, parameters $D_{s,c}$ and k_c have large variances and are unidentifiable in Case 2- SC_4 while these parameters become identifiable in Case 3- SC_4 . These results confirm observations obtained from the sensitivity analysis presented in Figures 11 and 12. We can also conclude that voltage and electrolyte concentration at a single location is sufficient to reliably identify 90% of the

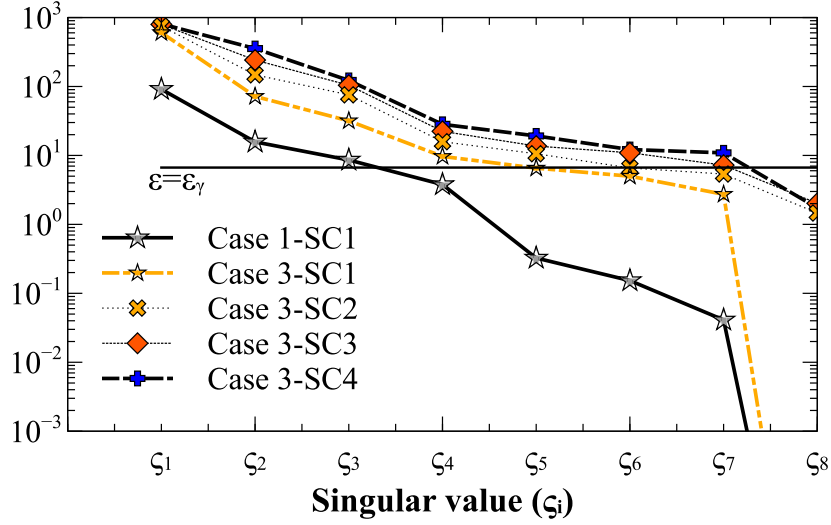


Figure 10: Case 3: Spectrum of singular values under different scenarios.

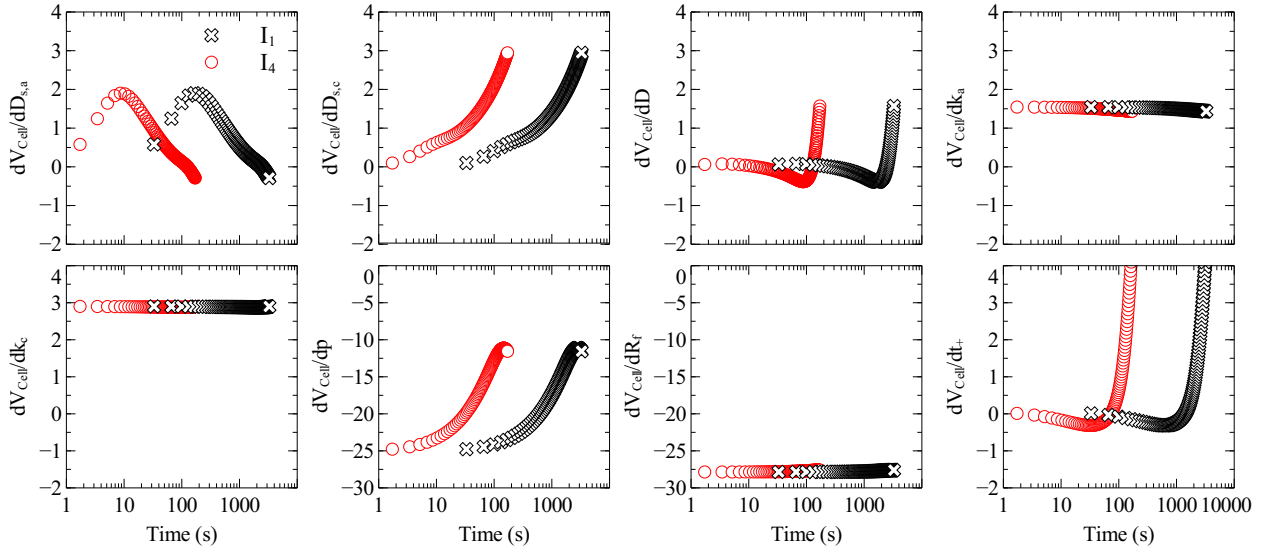


Figure 11: Sensitivity time profiles of cell voltage with respect to parameters $dV_{cell}(t)/d\theta$ at nominal I_1 and fast I_4 discharge rates for scenario Case 3-SC4.

parameters.

An intriguing finding of our study is that the anode reaction constant k_a remains highly unstable, despite the addition of electrolyte concentration information. This is particularly evident from the marginal pdfs presented in Figure 11. This is also confirmed by the spectrum analysis which gives only seven well-conditioned singular values. From the sensitivity profiles we can see that this parameter indeed excites the output variables. This, however, does not seem sufficient to reliably estimate the parameter. This situation can be explained from the observations made by Ramadesigan, et.al., [37]; who note that very strong variations (orders of magnitude) of the anode reaction constant are

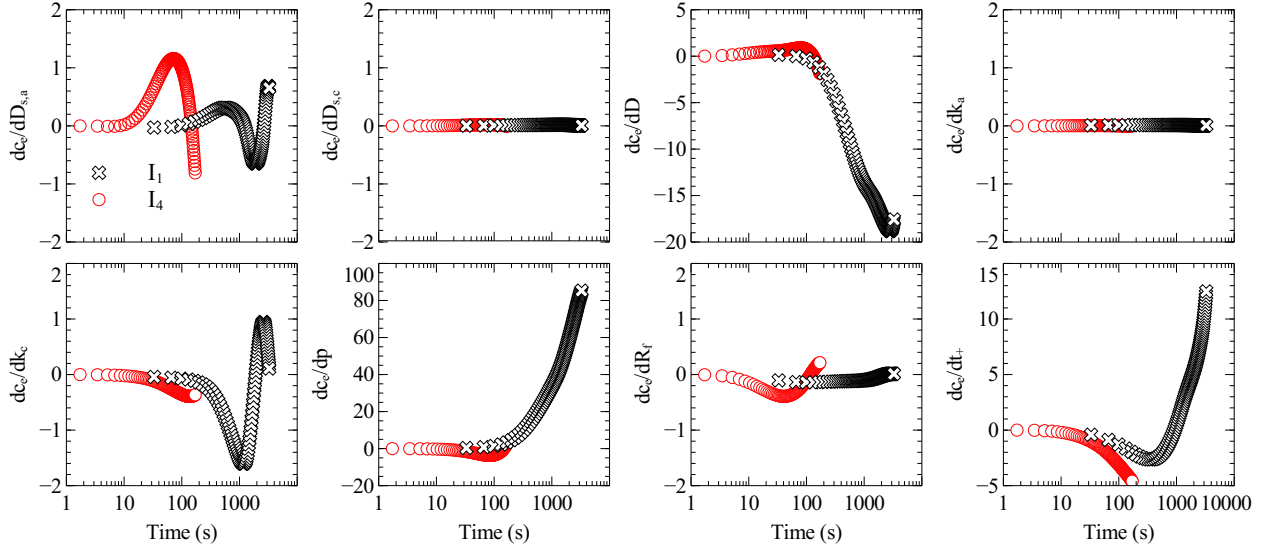


Figure 12: Sensitivity time profiles of electrolyte concentration in the separator with respect to parameters $dc_e(\ell_a + \ell_s/2, t)/d\theta$ at nominal I_1 and fast I_4 discharge rates for scenario Case 3- SC_4 .

needed to have an impact on the voltage curve. Our results indicate that, at its nominal value, this parameter has little influence on the discharge curve. It is possible, however, that around another nominal point such insensitivity disappears. We will explore this issue in future work.

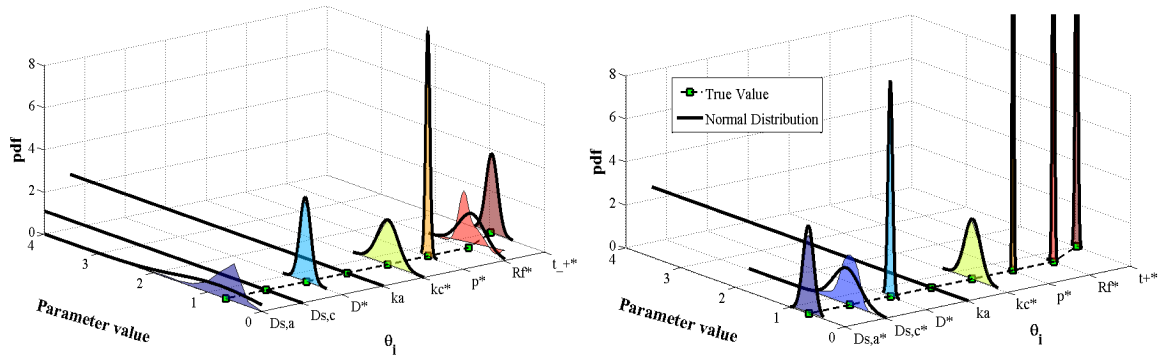


Figure 13: Case 3: Marginal pdfs for scenarios Case 3- SC_1 (left) and Case 3- SC_4 (right).

4.4 Computational Issues

The PDAE system is implemented in Matlab and is discretized by using 11 points in the axial direction for each region and 11 points for the radial direction. We use the discretization routines `ds010` and `ds044` as in [34]. The resulting DAE system contains 561 equations and is solved by using the integrator IDAS from SUNDIALS which provides forward and adjoint sensitivity analysis capabilities [22]. The parameter estimation problems are solved using the nonlinear least-squares routine `lsqnonlin` of Matlab (we use the trust region reflective algorithm). All results were obtained on a

Intel (R) Core(TM) i7-4770K CPU running at 3.50GHz and with 32.0 GB of available RAM memory.

The computational results are summarized in Table 10. The average simulation time was in the range of 3-7 seconds except for the slow discharge rate which required 48 seconds. This is because the slow discharge rate requires a long integration time to reach the cut-off voltage. The number of iterations required to solve the parameter estimation problems is decreased as we add experimental information because the problem becomes better conditioned and the optimization algorithm can more easily identify a solution. The only exception is instance Case 2- SC_6 , which increases the number of iterations. We attribute this to the lack of information introduced by scenario SC_6 at slow discharge rates. The solution times for Case 2 are longer than those of Case 3 because the latter requires the computation of additional sensitivity information. A Monte Carlo procedure with 200 replications for Case 3- SC_4 currently requires around two days to complete. We note, however, that these replications can be performed in parallel and can potentially reduce the time down to fifteen minutes. In addition, simulations for estimation problems with multiple experiments can also be performed in parallel. For Case 3- SC_4 this could reduce the time to four minutes. Parallel parameter estimation approaches have been proposed in [13, 52]. We will also investigate the use of reduced models, as those proposed in [37].

Table 10: Computational results for simulation and parameter estimation problems.

Simulation		Estimation		
Discharge Rate	Time [seconds]	Instance	Time [seconds]	Iterations
1.0 C	6.1	Case 2- SC_1	476.6	73
2.0 C	5.4	Case 2- SC_2	711.8	54
3.0 C	4.3	Case 2- SC_3	520.6	31
4.0 C	3.6	Case 2- SC_4	343.6	18
0.5 C	6.6	Case 2- SC_6	3751.8	32
0.1 C	48.1	Case 3- SC_1	388.8	70
		Case 3- SC_2	664.0	57
		Case 3- SC_4	915.2	47

5 Conclusions and Future Work

We have presented a computational framework that combines sensitivity and Monte Carlo to evaluate quality of parameter estimates and diagnose ill-conditioning and identifiability issues. Our analysis indicates that voltage profile information collected from discharge experiments only enables the estimation of a small parameter subset. The incorporation of electrolyte concentration profiles at a single axial point is sufficient to estimate seven of eight parameters: the Li^+ diffusion coefficient in the solid particle of anode, the Li^+ diffusion coefficient in the solid particle of cathode, the salt diffusion coefficient in the electrolyte, the reaction rate constant in the cathode, the Bruggman coefficient, the film resistance at the anode, and the transport number. The only unidentifiable parameter is the reaction rate constant in the anode. We demonstrate that sensitivity methods can qualitative

identify unidentifiable parameters using only structural information of the sensitivity matrix. This provides an advantage over the most rigorous but also more expensive Monte Carlo method. As part of future work, we will use our framework to investigate impacts of other sources of experimental information on identifiability and ill-conditioning. We will also develop an implementation tailored to high-performance computing architectures to accelerate analysis times.

Acknowledgments

This work was supported by the U.S. Department of Energy, under Contract No. DE-AC02-06CH11357 and the Collaborative Research Center SFB/TR 63 InPROMPT "Integrated Chemical Processes in Liquid Multiphase Systems" both coordinated by the Technische Universität Berlin and funded by the German Research Foundation (Deutsche Forschungsgemeinschaft DFG). Diana C. López C. gratefully acknowledges the financial support from the German Academic Interchange Service (DAAD) for a doctoral stipend.

References

- [1] S. P. Asprey and S. Macchietto. Statistical tools for optimal dynamic model building. *Computers & Chemical Engineering*, 24(2):1261–1267, 2000.
- [2] Y. Bard. *Nonlinear parameter estimation*. Academic Press, New York, 1974.
- [3] T. Barz, S. Kuntsche, G. Wozny, and H. Arellano-Garcia. An efficient sparse approach to sensitivity generation for large-scale dynamic optimization. *Computers & Chemical Engineering*, 35(10):2053–2065, 2011.
- [4] D. A. Belsley. *Conditioning diagnostics: Collinearity and weak data in regression*. John Wiley & Sons, New York, USA, 1991.
- [5] D. A. Belsley, E. Kuh, and R. E. Welsch. *Regression diagnostics: Identifying influential data and sources of collinearity*. John Wiley & Sons, New York, USA, 1980.
- [6] R. Brun, M. Kühni, H. Siegrist, W. Gujer, and P. Reichert. Practical identifiability of asm2d parameters - systematic selection and tuning of parameter subsets. *Water Research*, 36(16):4113–4127, 2002.
- [7] M. Burth, G. C. Verghese, and M. Vélez-Reyes. Subset selection for improved parameter estimation in on-line identification of a synchronous generator. *Power Systems, IEEE Transactions on*, 14(1):218–225, 1999.
- [8] Y. Chu and J. Hahn. Parameter set selection via clustering of parameters into pairwise indistinguishable groups of parameters. *Industrial & Engineering Chemistry Research*, 48(13):6000–6009, 2008.

- [9] Y. Chu and J. Hahn. Generalization of a parameter set selection procedure based on orthogonal projections and the d-optimality criterion. *AIChE Journal*, 58(7):2085–2096, 2012.
- [10] C. Cobelli and J. J. DiStefano. Parameter and structural identifiability concepts and ambiguities: a critical review and analysis. *American Journal of Physiology-Regulatory, Integrative and Comparative Physiology*, 239(1):R7–R24, 1980.
- [11] M. Doyle, T. F. Fuller, and J. Newman. Modeling of galvanostatic charge and discharge of the lithium/polymer/insertion cell. *Journal of the Electrochemical Society*, 140(6):1526–1533, 1993.
- [12] M. Doyle, J. Newman, A. S. Gozdz, C. N. Schmutz, and J.M. Tarascon. Comparison of modeling predictions with experimental data from plastic lithium ion cells. *Journal of the Electrochemical Society*, 143(6):1890–1903, 1996.
- [13] R. Faber, P. Li, and G. Wozny. Sequential parameter estimation for large-scale systems with multiple data sets: 1. computational framework. *Ind. Eng. Chem. Res.*, 42:5850–5860, 2003.
- [14] J. A. Fessler. Mean and variance of implicitly defined biased estimators (such as penalized maximum likelihood): Applications to tomography. *Image Processing, IEEE Transactions on*, 5:493–506, 1996.
- [15] J. C. Forman, S. J. Moura, J. L. Stein, and H. K. Fathy. Genetic parameter identification of the doyle-fuller-newman model from experimental cycling of a lifepo 4 battery. In *American Control Conference (ACC), 2011*, pages 362–369. IEEE, 2011.
- [16] Joel C Forman, Scott J Moura, Jeffrey L Stein, and Hosam K Fathy. Genetic identification and fisher identifiability analysis of the doyle–fuller–newman model from experimental cycling of a lifepo 4 cell. *Journal of Power Sources*, 210:263–275, 2012.
- [17] G. Franceschini and S. Macchietto. Model-based design of experiments for parameter precision: State of the art. *Chemical Engineering Science*, 63(19):4846–4872, 2007.
- [18] Alejandro A Franco. Multiscale modelling and numerical simulation of rechargeable lithium ion batteries: concepts, methods and challenges. *RSC Advances*, 3(32):13027–13058, 2013.
- [19] T. F. Fuller, M. Doyle, and J. Newman. Simulation and optimization of the dual lithium ion insertion cell. *Journal of the Electrochemical Society*, 141(1):1–10, 1994.
- [20] G. H. Golub and C. F. Van Loan. *Matrix computations*, volume 3. Johns Hopkins University Press, 1996.
- [21] A. Grah. *Entwicklung und Anwendung modularer Software zur Simulation und Parameterschätzung in gaskatalytischen Festbettelektrolytoren*. PhD thesis, Martin Luther University Halle-Wittenberg, 2004.
- [22] A. C. Hindmarsh, P. N. Brown, K. E. Grant, S. L. Lee, R. Serban, D. E. Shumaker, and C. S. Woodward. Sundials: Suite of nonlinear and differential/algebraic equation solvers. *ACM Transactions on Mathematical Software (TOMS)*, 31(3):363–396, 2005.

- [23] A. E. Hoerl and R. W. Kennard. Ridge regression: Biased estimation for nonorthogonal problems. *Technometrics*, 12:55–67, 1970.
- [24] Y. Hu, S. Yurkovich, Y. Guezennec, and B. J. Yurkovich. A technique for dynamic battery model identification in automotive applications using linear parameter varying structures. *Control Engineering Practice*, 17(10):1190–1201, 2009.
- [25] E. A. Jacobson. *A statistical parameter estimation method using singular value decomposition with application to Avra Valley aquifer in southern Arizona*. PhD thesis, The University of Arizona, 1985.
- [26] C. Kravaris, J. Hahn, and Y. Chu. Advances and selected recent developments in state and parameter estimation. *Computers & Chemical Engineering*, 51:111–123, 2013.
- [27] L. Lennart and P. E. Caines. Asymptotic normality of prediction error estimators for approximate system models. *Stochastics*, 3(1-4):29–46, 1980.
- [28] Y. C. Liang, H. P. Lee, S. P. Lim, W. Z. Lin, K. H. Lee, and C. G. Wu. Proper orthogonal decomposition and its applications -part i: Theory. *Journal of Sound and Vibration*, 252(3):527–544, 2002.
- [29] D. C. López C., T. Barz, S. Körkel, and G. Wozny. Nonlinear ill-posed problem analysis in model-based parameter estimation and experimental design. *Computers & Chemical Engineering*, 51:111–123, 2015.
- [30] D. C. López C., T. Barz, M. Peñuela, A. Villegas, S. Ochoa, and G. Wozny. Model-based identifiable parameter determination applied to a simultaneous saccharification and fermentation process model for bio-ethanol production. *Biotechnology Progress*, 29(4):1064–1082, 2013.
- [31] Rodrigo López-Negrete and Lorenz T Biegler. A moving horizon estimator for processes with multi-rate measurements: A nonlinear programming sensitivity approach. *Journal of Process Control*, 22(4):677–688, 2012.
- [32] T. Maly and L. R. Petzold. Numerical methods and software for sensitivity analysis of differential-algebraic systems. *Applied Numerical Mathematics*, 20(1):57–79, 1996.
- [33] D. W. Marquardt. Generalized inverses, ridge regression, biased linear estimation, and nonlinear estimation. *Technometrics*, 12:591–612, 1970.
- [34] E. Martínez-Rosas, R. Vasquez-Medrano, and A. Flores-Tlacuahuac. Modeling and simulation of lithium-ion batteries. *Computers & Chemical Engineering*, 35(9):1937–1948, 2011.
- [35] K. A. P. McLean, S. Wu, and K. B. McAuley. Mean-squared-error methods for selecting optimal parameter subsets for estimation. *Industrial & Engineering Chemistry Research*, 51:6105–6115, 2012.
- [36] F. Pukelsheim. *Optimal design of experiments*. Wiley, New York, 1 edition, 1993.

- [37] Venkatasailanathan Ramadesigan, Vijayasekaran Boovaragavan, Mounika Arabandi, Kejia Chen, Hisashi Tsukamoto, Richard Braatz, and Venkat Subramanian. Parameter estimation and capacity fade analysis of lithium-ion batteries using first-principles-based efficient reformulated models. *ECS Transactions*, 19(16):11–19, 2009.
- [38] Venkatasailanathan Ramadesigan, Kejia Chen, Nancy A Burns, Vijayasekaran Boovaragavan, Richard D Braatz, and Venkat R Subramanian. Parameter estimation and capacity fade analysis of lithium-ion batteries using reformulated models. *Journal of The Electrochemical Society*, 158(9):A1048–A1054, 2011.
- [39] Venkatasailanathan Ramadesigan, Paul WC Northrop, Sumitava De, Shriram Santhanagopalan, Richard D Braatz, and Venkat R Subramanian. Modeling and simulation of lithium-ion batteries from a systems engineering perspective. *Journal of The Electrochemical Society*, 159(3):R31–R45, 2012.
- [40] Shriram Santhanagopalan, Qingzhi Guo, and Ralph E White. Parameter estimation and model discrimination for a lithium-ion cell. *Journal of the Electrochemical Society*, 154(3):A198–A206, 2007.
- [41] A. P. Schmidt, M. Bitzer, Á. W. Imre, and L. Guzzella. Experiment-driven electrochemical modeling and systematic parameterization for a lithium-ion battery cell. *Journal of Power Sources*, 195(15):5071–5080, 2010.
- [42] A. Sharma and H. K. Fathy. Fisher identifiability analysis for a periodically-excited equivalent-circuit lithium-ion battery model. In *American Control Conference (ACC), 2014*, pages 274–280. IEEE, 2014.
- [43] V. R. Subramanian, V. Boovaragavan, V. Ramadesigan, and M. Arabandi. Mathematical model reformulation for lithium-ion battery simulations: Galvanostatic boundary conditions. *Journal of The Electrochemical Society*, 156(4):A260–A271, 2009.
- [44] S. Vajda, H. Rabitz, E. Walter, and Y. Lecourtier. Qualitative and quantitative identifiability analysis of nonlinear chemical kinetic models. *Chemical Engineering Communications*, 83:191–219, 1989.
- [45] V. S. Vassiliadis, E. B. Canto, and J. R. Banga. Second-order sensitivities of general dynamic systems with application to optimal control problems. *Chemical Engineering Science*, 54(17):3851–3860, 1999.
- [46] M. Velez-Reyes and G. C. Verghese. Subset selection in identification, and application to speed and parameter estimation for induction machines. In *Proceedings of the 4th IEEE Conference on Control Applications*, pages 991–997, Albany, 1995.
- [47] E. Walter and L. Pronzato. On the identifiability and distinguishability of nonlinear parametric models. *Mathematics and Computers in Simulation*, 42:125–134, 1996.

- [48] E. Walter and L. Pronzato. *Identification of parametric models*. Springer, New-York, USA, 1997.
- [49] S. R. Weijers and P. A. Vanrolleghem. A procedure for selecting best identifiable parameters in calibrating activated sludge model no. 1 to full-scale plant data. *Water science and technology*, 36:69–79, 1997.
- [50] S. Wu, K. A. P. McLean, T. J. Harris, and K. B. McAuley. Selection of optimal parameter set using estimability analysis and mse-based model-selection criterion. *International Journal of Advanced Mechatronic Systems*, 3:188–197, 2011.
- [51] K. Z. Yao, B. M. Shaw, B. Kou, K. B. McAuley, and D. W. Bacon. Modeling ethylenebutene copolymerization with multi-site catalysts parameter estimability and experimental design. *Polymer Reaction Engineering*, 11:563–588, 2003.
- [52] V. M. Zavala, C. D. Laird, and L. T. Biegler. Interior-point decomposition approaches for parallel solution of large-scale nonlinear parameter estimation problems. *Chemical Engineering Science*, 63(19):4834–4845, 2008.
- [53] Victor M Zavala. *Computational strategies for the optimal operation of large-scale chemical processes*. ProQuest, 2008.

This material is based upon work supported by the U.S. Department of Energy, Office of Science, under contract number DE-AC02-06CH11357.

The submitted manuscript has been created by the University of Chicago as Operator of Argonne National Laboratory (“Argonne”) under Contract No. DE-AC02-06CH11357 with the U.S. Department of Energy. The U.S. Government retains for itself, and others acting on its behalf, a paid-up, nonexclusive, irrevocable worldwide license in said article to reproduce, prepare derivative works, distribute copies to the public, and perform publicly and display publicly, by or on behalf of the Government.